A CHEMICALLY REACTING, TURBULENT SHEAR LAYER

Thesis by

Robert Edward Breidenthal, Jr.

In Partial Fulfillment of the Requirements

For the Degree of

Doctor of Philosophy

California Institute of Technology

Pasadena, California

1979

(Submitted November 15, 1978)

ACKNOWLEDGMENTS

Any increment of understanding builds upon the foundation laid by predecessors. To paraphrase Newton, the view is clearest from the shoulders of giants. This work is the direct result of the ideas, assistance and inspiration of many people. Drs. James E. Broadwell, Garry L. Brown, Paul E. Dimotakis, John H. Konrad, Frank E. Marble, Phillip G. Saffman and Mr. Luis P. Bernal were valuable sources of ideas. There were productive discussions with essentially everyone in the department.

I am grateful for the assistance of a host of people: Earl Dahl and the supporting shops for their technical advice, Betty Wood for her draftsmanship, Jackie Beard, Marcia Clark and Kathy Franson for typing the thesis, Til Liepmann for his help in the summer, and the Astronomy Department for the use of their microphotometer. The generous financial assistance of the Donald Douglas and NSF Fellowships is gratefully acknowledged. The research was sponsored by AFOSR Contract No. F44620-76-C-0046.

Professors Anatol Roshko and Hans W. Liepmann were sources not only of ideas, but inspiration. Their long-term enthusiasm was unperturbed by short term obstacles, no matter how titanic they appeared to me from down in the subbasement.

Finally, I want to thank my wife Cathy for her patience and our son Matthew for reminding me of curiosity.

ABSTRACT

A chemically reacting turbulent shear layer was investigated in a new, blow-down water tunnel. In a diffusion-limited reaction, a pH indicator, phenolphthalein, in one stream mixed and reacted with a base, sodium hydroxide, in the other stream to form a visible reaction product. Using optical densitometry techniques, the amount of product was measured as a function of Reynolds number, at a relatively high Schmidt number of approximately 600. The results were compared with both the previous mixing measurements of Konrad in a gaseous shear layer ($Sc \doteq 0.7$) and the simple mixing model of Broadwell.

The product was found to be distributed, as expected, in concentrated lumps associated with the large, spanwise-coherent structures of the turbulence. The time averaged amount of product in the layer exhibited a rapid transition at a large-structure Reynolds number of about 5×10^3 for a velocity ratio of 0.38. Above the transition, the amount of product within the layer was independent of Reynolds number.

This transition is related to the introduction of small scale, three-dimensional motions into the layer. In the initial region, where the flow was already unsteady and contained large structures but was strictly two-dimensional, very little mixing was observed. Downstream the flow became unstable to three-dimensional perturbations and small scale, three-dimensional motions were introduced into the layer. Across this transition, the aqueous mixing increased by an order of magnitude, indicating the sensitivity of mixing to small scales

of the turbulence in a high Schmidt number fluid. At high Reynolds numbers, changing the Schmidt number by three orders of magnitude only altered the molecular mixing by about a factor of two or less. The mixing model of Broadwell, which addresses the effect of Schmidt number, is in satisfactory qualitative agreement with the observations.

The unique flow visualization of the visible reaction product in water permitted a study of the three-dimensional instability and evolution of small scale motions in the layer. Streamwise streaks which had been previously observed in the Brown-Roshko gas apparatus were found to originate from a spanwise-sinuous wiggle which appeared at a large-structure Reynolds number which varied with velocity ratio, indicating an influence of initial conditions on the instability.

TABLE OF CONTENTS

TABLE OF CONTENTS (Cont'd.)

LIST OF SYMBOLS

A - reactant

B - reactant

C - reaction product

$\mathcal{D}$ - coefficient of diffusivity

d - trailing edge thickness of splitter plate

f - equivalence ratio

f* - stoichiometric ratio

ℓ - spacing between large structures

P - equivalent product thickness (Eq. 4.1)

Re - large-structure Reynolds number $\frac{\Delta U \delta}{\nu}$

Sc - Schmidt number $\frac{\nu}{\mathcal{D}}$

r - velocity ratio (U_2/U_1)

t - time

T - Broadwell Mixing Parameter $\frac{Sc}{(Re)^{\frac{1}{2}}}$

U - velocity component in streamwise direction

u' - streamwise velocity fluctuation

v' - orthogonal velocity fluctuation

x - streamwise coordinate

y - orthogonal coordinate

z - spanwise coordinate

ΔU - $U_1 - U_2$

δ - shear layer thickness, maximum slope of mean velocity profile (Eq. 5.1)

δ_w - wake thickness (Eq. 5.3)

η - diffusion similarity variable $\frac{y}{(\nu t)^{\frac{1}{2}}}$

θ - boundary layer momentum thickness

λ_o - Kolmogorov microscale

ν - kinematic viscosity

ξ - diffusion interface thickness

σ - strain rate

τ - characteristic time scale

$\underline{\omega}$ - vorticity vector

LIST OF FIGURES

I. INTRODUCTION

Turbulent shear layers have been studied at the California Institute of Technology for more than a decade. Mixing in these flows has recently been measured in order to understand more fully the fluid mechanics of the turbulence as well as to address important technological questions. This work is a continuation of previous experiments, the main difference being the study of a chemically reacting flow in a fluid with a relatively high Schmidt number. Schmidt number ($Sc \equiv \frac{\nu}{\mathcal{D}}$) is the ratio of the diffusion coefficient of vorticity to that of species.

The mixing in a two-dimensional, turbulent shear layer produced by two aqueous streams flowing parallel to each other at different speeds was studied (see Figure 1). The goal was to determine the amount and distribution of molecular scale mixing within the layer, as a function of Reynolds number and, to a limited degree, Schmidt number.

The particular flow geometry was chosen for several reasons. The flow is well documented and similar to the situation in many non-premixed, continuous flow chemical reactors. Further, a turbulent shear layer is perhaps the simplest turbulent flow. Both the initial vorticity and the geometry are two-dimensional, and the initial vorticity is essentially of one sign.

Previous work had established that the plane shear layer consisted of large, basically two-dimensional vortical structures which dominate the flow (Brown and Roshko, 1974). These large structures have been found to persist at all observed Reynolds

numbers (Brown and Dimotakis, 1976). As the Reynolds number increased, smaller scale, three-dimensional motions appeared which were superimposed upon the ubiquitous large structures. In a gaseous mixing layer with Sc ~ 0.7, Konrad (1976) reported that the molecular mixing was independent of Reynolds number except for a transition region where the smaller scale, three-dimensional motions were introduced into the layer. At the transition the gaseous mixing increased by about 25%, according to Konrad's measurements.

The simple mixing model proposed by Broadwell (see Witte, et al., 1974) visualizes the mixing process as a sequence of events. The first step is the entrainment of pure, irrotational fluid into the layer. The entrained lump of fluid is subsequently broken down into smaller and smaller scales until finally the smallest scale is reached, the Kolmogorov microscale. If diffusion is slow enough, then diffusion across the microscale will be the bottleneck in the sequence of events which culminate in molecular scale mixing. The mixing is then small scale diffusion limited.

In the case of relative rapid diffusion at the Kolmogorov microscale, the model predicts that the mixing is limited by entrainment. Entrainment is visualized, following Brown and Roshko (1974), as the large scale engulfment of irrotational fluid by the large vortical structures. These structures are assumed to behave in an inviscid manner, independent of Reynolds number; thus entrainment is also independent of Reynolds number. If diffusion is rapid enough, entrainment is the slow step in the mixing process. The mixing is then entrainment limited and independent of Reynolds number and

Schmidt number.

The time to diffuse across the microscale λ_o is $\tau_{\lambda_o} \sim \frac{\lambda_o^2}{\mathcal{D}}$ where $\mathcal{D}$ is a species diffusion coefficient. The entrainment time τ_δ is

$$\tau_\delta \sim \frac{\delta}{\Delta U}$$

where δ is the large scale and ΔU is the velocity jump across the layer ($\Delta U = U_1 - U_2$). The ratio of these two time scales is

$$T \equiv \frac{\tau_{\lambda_o}}{\tau_\delta} \sim \frac{Sc}{Re^{\frac{1}{2}}} \quad , \quad \text{where } Re \equiv \frac{\Delta U \delta}{\nu} \; .$$

This model predicts that when the time parameter $T \gg 1$, the mixing is limited by small scale diffusion whereas for $T \ll 1$, large scale entrainment is the slow process. In the entrainment-limited regime ($T \ll 1$), the mixing should be independent of Re and Sc. At some intermediate value of T, a transition region must exist. The results of Konrad (1976) with $T \sim 10^{-2}$, are consistent with the model for $T \ll 1$.

The amount of mixing should be very sensitive to the smallest scales when the mixing is small-scale diffusion limited. Therefore, the mixing could be viewed as a sensitive probe of the behavior of the small scales at low Reynolds numbers.

The original aims of this research were as follows:

1) Measure the amount and distribution of mixing in the plane shear layer as a function of Reynolds number in a large Schmidt number fluid.

2) Compare the results with Konrad's measurements which

were made in a near-unity Schmidt number fluid; i.e., a gas.

3) Test Broadwell's model.

4) Utilize the small scale sensitivity and resolution inherent in high Schmidt number flows to investigate the small scale motions of the turbulence.

II. EXPERIMENTAL FACILITY AND INSTRUMENTATION

2.1 Design Philosophy and Flow Apparatus

The experiments were performed in a new water tunnel designed to produce a turbulent shear layer between two streams of aqueous solutions. The design philosophy was to construct a simple, general purpose apparatus which could be operated by one person and easily modified to vary the test section flow conditions. In order to test Broadwell's model, a large scale Reynolds number of at least $\frac{\Delta U \delta}{\nu} = 10^4$ was desirable. For a fixed velocity ratio, Re goes like the characteristic test section dimension, while the volume flow rate goes like its square. In the interest of conserving reactant chemicals, the test section was sized to be relatively small, 7 cm x 11 cm span x 45 cm long. With a design speed of 300 cm/sec, the goal of Re = 10^4 was achieved with a relatively small expenditure of reactant chemicals.

Since the reactants would mix and react in the test section, a closed circuit tunnel was not feasible. Rather, a blow-down configuration was chosen, with the reactant solutions prepared in batches before a run and the waste water treated and thrown away afterwards.

To achieve accurate and repeatable flow speeds over a range from about 1 to 300 cm/sec requires exquisite pressure regulation. The dynamic head of a 1 cm/sec flow is only 5 microns of water, while the volume flow rate of one stream through the test section at 300 cm/sec is 12 liters per second. These are formidable specifications for a pressure regulator, so a much simpler system was adopted. By allowing gravity to supply the head, and using valves to throttle the flow, the apparently incompatible requirements of accurate

regulation and large capacity were resolved.

A gravity driven apparatus could either maintain a constant water level (and head) using weirs or the head could decrease during the run as the water level fell. The possibly adverse health effects of waterfalls and mists of corrosive fluids discouraged the former option. The penalty of a decreasing head during a run could be minimized by building reservoirs with large surface areas. (An infinite surface area reservoir would maintain constant head but would be difficult to construct.) Since the flow speed goes like the square root of the head, the decline in speed is relatively less than the change in head. In addition, throttling valves that restrict the flow further minimize the variation in flow speed due to changes in water level.

When the water levels fall to near the bottom of the reservoirs during a run, air may be (undesirably) ingested into the apparatus due to either an irrotational, potential flow out the reservoir drain* or a bathtub vortex there. The radius of the drain inlets was designed, following Zukoski (see Gluck et al.,1966) to inhibit irrotational air inhalation, and guide vanes were incorporated to discourage bathtub vortex formation.

The height of the reservoirs above the apparatus was chosen so that considerable excess head was available for dissipation in turns, settling chambers, honeycomb and screens. The head required for the design speed (300 cm/sec) is 45 cm while the reservoirs are located one floor above the test section ($\sim$ 300 cm). Thus over 200 cm of head is available for dissipation.

*Suggested by Professor E. E. Zukoski

A sketch of the apparatus is shown in Figure 2. Each reservoir has a capacity of about 10^3 liters, permitting a 30 second long run at the design speed of 300 cm/sec. Due to the relatively small change in water level, the flow speed changes by less than 2% in 10 seconds. Steady state flow is typically established in 2-4 seconds. The free-stream turbulence intensity $\frac{\sqrt{\overline{u'^2}}}{\overline{U}}$ was measured by a laser doppler velocimeter* to be slightly less than 0.5% at the beginning of the test section.

The apparatus was designed to handle a variety of corrosive, aqueous solutions. For example, one of the chemicals used in the present work, sodium hydroxide, attacks glass. Thus the test section windows were all fabricated out of lucite, and the bulk of the apparatus was built of polyvinyl chloride (PVC). PVC is very inert, yet can be joined together with a cement. Easily replaceable parts were machined from 316 or 304 stainless steel where additional rigidity was required.

Figure 3 is a photograph of the apparatus. The white vertical pipes which drain the overhead tanks one floor above (not shown) are visible at the left of the picture. The lucite test section in the middle and the large catch tank at the far right are also apparent. Figure 4 is a close up of the contraction and test section. The thin splitter plate makes a timid appearance at the left, or upstream, end of the test section.

The settling chambers were designed to permit the rapid

*with the help of Mr. Manooch Mohseni-Koochesfahani and Mr. Keith Koenig

exchange of "turbulence manipulators" (e.g., honeycomb, screens, etc.). The screens were mounted on frames which were stacked in the desired sequence and placed within the settling chambers. Removal of a rear cover plate readily gains access to both settling chambers.

The contraction was modelled after the one in the Brown-Roshko gas apparatus except that the contraction ratio was increased from 4 to 6. A rapid contraction is used to accelerate the flow and minimize the thickness of the splitter plate boundary layers. A contraction ratio of six results in relatively low flow speeds through the settling chamber so that the pressure drop across the screens is acceptable.

The dimensions of the contraction are indicated in Figure 5. The nozzle contour is defined by two circular arcs. The "thin" splitter plate is a wedge whose trailing edge thickness is less than .003 cm. A "thick" splitter plate, used for some wake measurements, is a truncated wedge of the same length whose trailing edge thickness is 0.635 cm.

All four walls of the horizontal test section are transparent so that the flow can be observed from any direction. The side walls are easily replaceable with ones of a different convergence angle, to adjust and remove any streamwise pressure gradients.

A stainless steel traversing mechanism, driven by a digitally controlled stepping motor, could move a pitot tube probe at 500 steps per second in increments of 0.0066 cm across the test section.

2.2 Instrumentation

2.2a Manometer System

Test section velocities were calculated from total and static pressure measurements. The thickness and growth rate of the layer were measured by pitot tube traverses. Test section pressure gradients were measured from a row of static taps on the side walls. The pressure measuring system consisted of a fast pressure scanner switch (Scanivalve, type W1260), a fluid isolator (Datametrics, 552), a pressure transducer (Datametrics electronic manometer, 1014A) and a differential pressure sensor (Datametrics, 511-10). Total and static pressure lines were sequentially sampled by the Scanivalve switch. The isolator prevented the electrically conductive reactant solution within the pressure lines from entering the capacitive diaphram pressure transducer. Within the isolator, the pressure signal was transmitted from the reactant fluid across a thin, flexible membrane to a dielectric oil which filled the transducer.

The Scanivalve switch was automatically actuated by a digital master control. The analog output of the manometer was read by a digital voltmeter and written by a printer at a rate of 3 readings per second. With each pressure reading the Scanivalve position was also encoded by the printer. In this way, up to 12 different pressure lines could be sequentially sampled and the corresponding pressures recorded.

2.2b Optical System

The concentration of the visible reaction product was measured

using two densitometric techniques. The first approach employed a photographic film emulsion as the measuring device.* This involved photographing the reacting flow through a green filter and scanning the photographic negative. The absorption of green light by the red reaction product varied exponentially with the total amount of product along the light path. Photographic emulsions, within a certain exposure range, are logarithmic in nature. The net result is that the optical density of the negative was just a linear function of the total amount of reaction product along the light path. Thus, by photographing the reacting flow with a bright background and optically measuring the developed negative, it is possible to determine the amount of reaction product.

The virtue of the photographic technique is that a global measurement of the product is made. Past experience with turbulent flows (Brown and Roshko, 1974) strongly suggests that global view of the flow may be more instructive in recognizing large scale patterns than local point measurements. From a time exposure of the plan view of the layer, for example, spanwise variations in time averaged mixing are easily detected.

The disadvantages of the photographic technique are the inaccuracies associated with the film emulsion and non-uniform background lighting. These error sources limited the absolute accuracy of the measurements. Reasonable relative measurements can be made, however.

The second approach was adopted after the limitations of the

*Suggested by Dr. Paul E. Dimotakis

photographic technique became apparent. The attenuation by the red reaction product of a narrow beam of green light passing through the layer was measured (see Figure 6). With the beam oriented normal to the plane of the layer, the total amount of chemical product along the light path could be detected.

A mercury-argon discharge lamp (Pen-Ray, 11SC-1) produced a 5461 angstrom green mercury line near the phenolphthalein absorption maximum of 5530 angstrom. The detector was a photomultiplier tube (GE, 731 A). A narrow-band optical filter (35 angstrom half-maximum bandwidth) in front of the PM tube selected the appropriate mercury line. Apertures ranging in diameter from 150 to 2000 microns defined the beam width. At the very small apertures, a bright mercury arc lamp and collimating lens were used as the light source instead of the Pen-Ray lamp to produce a large enough detector signal.

The analog PM tube signal was amplified and digitized by a fast analog to digital converter (Preston, GMAD-3). The digital signal was temporarily stored in core memory of a calculator (Hewlett Packard, 9825A). The data were subsequently processed by the calculator and permanently stored on a magnetic tape cartridge.

III. METHOD

3.1 Passive Scalar Technique

The amount of molecular scale mixing in a turbulent shear layer between two streams can be measured in at least two ways. Perhaps the most obvious approach is the passive scalar contaminant technique illustrated in Figure 7. An inert scalar, for example a blue dye, is introduced into one stream. A diffusion interface always exists within the mixing layer which separates the blue fluid from the clear, undyed stream. Within the interface the blue dye diffuses into the clear fluid; thus all the molecular scale mixing occurs within the interface. If there were no diffusion, there would be essentially no molecular scale mixing, since, for a low Mach number flow, the smallest turbulent convective scales are enormous compared to any molecular dimension.

Using this technique the amount of blue dye within a small sampling volume is measured as a function of time. If the sampling volume is small enough to measure the true, local concentration of the dye, it is possible, using Toor's analysis (Toor, 1962) to infer the molecular scale mixing at that point. On the other hand, if the sampling volume is not small compared to the smallest concentration scales, i.e., the interface thickness, then the probe will smooth out the actual concentration fluctuations and thus overestimate the amount of mixing. The inert technique always yields an upper bound on the actual molecular scale mixing.

The diffusion interface can become quite thin in a high Schmidt number fluid like water. For typical high Reynolds number conditions in the present apparatus, the interface is estimated to

be as thin as the wavelength of light (see Appendix A). If so, it is impossible to construct even an optical sampling volume with dimensions small compared to the interface thickness. The interface could be several orders of magnitude thicker and still present a difficult problem experimentally. Of course, one could achieve a high Reynolds number flow by building a very large apparatus with a flow speed so low that the diffusion interface would be thick compared to an obtainable probe size. This approach, however, was not practical.

3.2 Chemical Reaction Technique

The problem of finite probe size would be solved if a process could be found which would measure the mixing at the molecular level and macroscopically display the correct answer independent of the interface thickness. Such a process is a second order chemical reaction: $A + B \rightarrow C$. If dilute reactant A is added to stream one, and B to stream two, and if they rapidly react when mixed at the molecular level to irreversibly form a reaction product C, then the amount of product formed is just equal to the amount of molecular scale mixing between the two streams at the reaction equivalence ratio. Further, if the reaction product happens to be visible, then the amount of mixing can be measured optically, in a non-obtrusive way.

In contrast to the passive case, the finite size of the sampling volume in the reacting flow does not inherently overestimate the amount of mixing (see Figure 8). If the reaction is "ideal" (see Section 3.3) then the total amount of mixed fluid within the sampling volume is just equal to the total amount of product there, no matter how big the sampling volume, or how thin the diffusion interface.

This attractive characteristic permits accurate aqueous mixing measurements at fairly high Reynolds numbers in a reasonably sized laboratory apparatus.

3.3 Chemical Considerations

The chemistry should be fast, so that there is no time delay between actual mixing and the formation of product. Diffusion-limited reactions are the fastest possible, in the sense that the time for two prospective reactant molecules to migrate toward each other is very long compared to the actual reaction time. A reaction occurs essentially every time two reactant molecules approach each other, so that molecular diffusion is the rate-limiting step. A consequence of a diffusion-limited reaction is that, in the continuum sense, the reactants cannot coexist.

There are two types of optimum, diffusion-limited chemical reactions for probing a turbulent flow. As has been mentioned, the first is an irreversible, second order reaction

$$A + B \rightarrow C.$$

The reaction product C is permanently formed by the reaction and represents the total, cumulative amount of molecular scale mixing of fluids containing A and B.

The second reaction (not employed in this work) is schematically

$$A + B \rightarrow C \overset{\tau}{\rightarrow} D.$$

Here C is formed when A and B mix, but after a short time, τ,

C disappears in some manner to form D. The intermediate product C now represents only the recent mixing, rather than the total, accumulated amount of mixing as in the first reaction. The short-lived product C would be useful for exploring regions of recent, active mixing in the turbulence.

The optimum chemical system for the first reaction was not found. Instead, this ideal, irreversible reaction has been approximated by a reversible one. Phenolphthalein, a common pH indicator, reacts with a base, sodium hydroxide, in a complex series of steps (Kolthoff, 1937). The overall reaction is

$$\text{Phenolphthalein} + 2(OH)^- \rightarrow \text{red product},$$

The reaction, while not the optimum*, was chosen for several reasons. It is believed to be diffusion-limited (Czerlinski and Eigen, 1959 and Caldin, 1964). The reactants are optically transparent while the product is visible. The reactants are more or less water soluble, non-toxic, and inexpensive. The red product is strongly visible so that dilute concentrations are sufficient for detection. Dilute reactants are unobtrusive so that the turbulence is unaffected by the reaction, i.e., little surface tension, buoyancy, heat release, etc.

Early in the investigation it was discovered that a precipitate formed upon the addition of sodium hydroxide to the water. The calcium and magnesium ions in the "hard" city water apparently were precipitating out as salts in the alkaline solution. An ion exchange water softener was installed to pretreat the water. It exchanged the

*Also see Appendix C.

troublesome calcium and magnesium with sodium ions. Sodium salts are much more soluble in alkaline solution and therefore did not precipitate out.

A typical run consisted of a long sequence of steps. Trapped bubbles of air within the apparatus were first flushed out. The valves were adjusted for the desired flow speeds. Concentrated reactant chemicals were then added to the reservoir tanks and the solutions thoroughly stirred. The base reservoir solution was adjusted to a pH of approximately 11.7 (see Appendix C) by adding concentrated sodium hydroxide of technical grade to the water. A phenolphthalein concentrate solution was prepared by dissolving reagent grade phenolphthalein powder in denatured ethanol. Then distilled water was added to form a 60% ethanol/40% water by volume solvent. The phenolphthalein concentrate was added to the water in the phenolphthalein reservoir tank to achieve a concentration of about 10^{-5} molar. Thus the equivalence ratio was the order of a few hundred, with an excess of $(OH)^-$.

The precise freestream concentration of phenolphthalein reactant was measured by the same optical system used to measure the red product formed in the test section during a run (see Figure 6). First a sample of the phenolphthalein reactant solution was diluted to 1/3 concentration with distilled water and raised to a pH of about 11.3 with sodium hydroxide. The diluted phenolphthalein reacted with the hydroxide ions $(OH)^-$ from the sodium hydroxide and turned bright red. The red solution was placed in a 1 cm optical path cuvette cell and the attenuation of green light through the cell was measured. The

measurement was repeated with an optically matched cell filled with distilled water. The difference between the two readings corresponded to the attenuation of 1/3 cm of reaction product.

The throttling valves were adjusted to the appropriate settings for the run. The valves were opened and the flow accelerated to final speed. After the settling chambers were flushed out by the fresh reactants, the shear layer became visible by the reaction product formed within it. After both the flow and the reactant concentrations stabilized within the test section, a computer program was initiated which automatically recorded 1000 photomultiplier readings at equal time intervals. Core memory limitations prevented a larger number of samples. The time interval was chosen to be large enough so that a repeatable time average of the product was obtained. After the data were recorded, the valves were closed to terminate the run.

To verify that the growth rate of the layer in this new apparatus was consistent with previous measurements in the Brown-Roshko gas facility (Brown and Roshko 1974, Konrad 1977) mean velocity profiles of the flow were measured. A small pitot tube was rapidly traversed across the layer The difference between the pitot pressure and the test section static pressure was measured by the differential manometer. The digital master control automatically drove the stepping motor to traverse the pitot tube across the flow and printed the manometer output. According to a preset frequency divider, the dynamic pressure was recorded after stepping the probe a preset number of times. Thus the increment in y between pressure

readings was known and adjustable. In this manner, the absolute thickness of the shear layer was measured.

3.4 Reaction Flow Visualization

A pleasant side effect of the visible reaction product was the unique flow visualization it afforded. The visualization technique had several advantages over conventional schemes. Chemical product was always being produced at the reaction interface so that it was always visible. If the interface was rapidly stretched, it was thinned and the reactant concentration gradients increased. The diffusive flux of reactants into the reaction surface thereby increased, producing more product per unit reaction surface area. In contrast, an inert dye or smoke injected into the flow at the splitter plate would have simply diffused away and eventually disappeared. With a reaction, new "dye" was continually being produced at the interface so that even far downstream the flow was readily visualized.

The slow diffusion rates of vorticity and matter in water are well known advantages in conventional flow visualization. Compared to typical gas facilities, water tunnels achieve large Reynolds numbers with relatively low flow speeds so that high speed photography is easier. In addition, the resolution of the photographs is superior since the aqueous species diffusion is so slow (e.g., the characteristic diffusion time across seven inches of water is about a year).

Perhaps the most useful feature of reacting flow visualization is the close relationship between vorticity and the visible product. Initially, the vorticity and product are both concentrated in thin

sheets at the splitter plate trailing edge. Both are convected with the flow and diffuse down concentration gradients (at different rates if $Sc \neq 1$). In a two-dimensional, constant density flow, vorticity is not stretched, and behaves just like a scalar contaminant, satisfying the Eulerian heat equation.

$$\frac{D\underline{\omega}}{Dt} = \nu\nabla^2\underline{\omega}$$

The local vorticity thickness, δ_{local}, for an isolated sheet in two-dimensional flow is just proportional to the local product thickness P (see Appendix B). The actual distributions of vorticity and product within the sheet are not identical, since product is continually being produced at the reaction surface, whereas

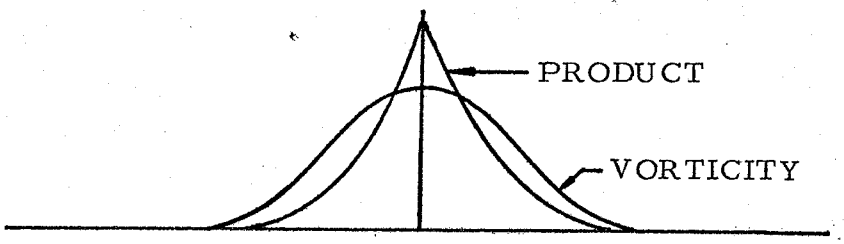

vorticity is not. (An inert dye would, however, label the vorticity provided $Sc = 1$.) Thus within the sheet, vorticity is not precisely labeled by product, even for a unity Schmidt number fluid.

As long as the sheet is isolated, i.e., its thickness is small compared to both its radius of curvature and the distance to any other nearby sheets, the maximum vorticity surface near the center of the sheet will approximately coincide with the reaction surface, the surface of maximum product. In this global sense, the product labels the vorticity for an isolated sheet, regardless of Schmidt number.

If the sheet is not isolated, "flame shortening" (Marble and Broadwell 1977) and "vortex sheet shortening" effects can alter the ratio $(P/\delta)_{local}$. And if the flow is three-dimensional, vortex stretching will amplify and rotate the vorticity vector. The chemical product is not amplified by stretching, of course, since it is a scalar.

In spite of the fact that the product does not precisely label the vorticity because of flame shortening and vorticity stretching effects, it may nonetheless approximately label it globally. Stretching only can amplify vorticity where vorticity already exists. One might argue that, for $Sc > 1$, vorticity can diffuse into an irrotational region faster than the product and then be amplified there by stretching to a very large absolute value. While such events must be common, if the Reynolds number is reasonably large the vorticity can not diffuse very far compared with the large scales in the turbulence. The viscous length is small and convection rather than diffusion dominates the transport of vorticity. From a global view, then, the chemical product may approximately label the vorticity.

IV. DATA REDUCTION

The green light beam was attenuated by the red reaction product as it passed through the reacting shear layer. The attenuation varied exponentially with the total amount of product along the light path. Since the photomultiplier (PM) tube signal was linearly related to the attenuation, the logarithm of the signal was just a linear function of the total amount of product along the beam. The slope of this line was computed from the attenuation of a known quantity of product. The PM tube signal for the beam passing through the test section full of clear water defined the zero product level.

After taking the logarithm of the recorded PM tube signal, a simple computer program computed the equivalent product thickness,

$$P(x, z, t) \equiv \int_{-\infty}^{\infty} \frac{[C](x, y, z, t)dy}{[B]_{\infty}} \qquad (4.1)$$

where $[C]$ is the product concentration and $[B]_{\infty}$ is the freestream concentration of reactant B (phenolphthalein). The product thickness P was defined as the intergral through the layer of the product concentration $[C](x, y, z, t)$ normalized by the freestream concentration of reactant B, the clear phenolphthalein. P has the dimensions of a length, and can be thought of as the equivalent thickness of a product layer with a uniform concentration equal to the freestream concentration of reactant B. For example, if the mean concentration profiles of the three species A, B, and C were as sketched, the equivalent mean product thickness, P, would be the height of a rectangle whose area equalled the area under the product profile and whose width

matched the freestream concentration, $[B]_\infty$.

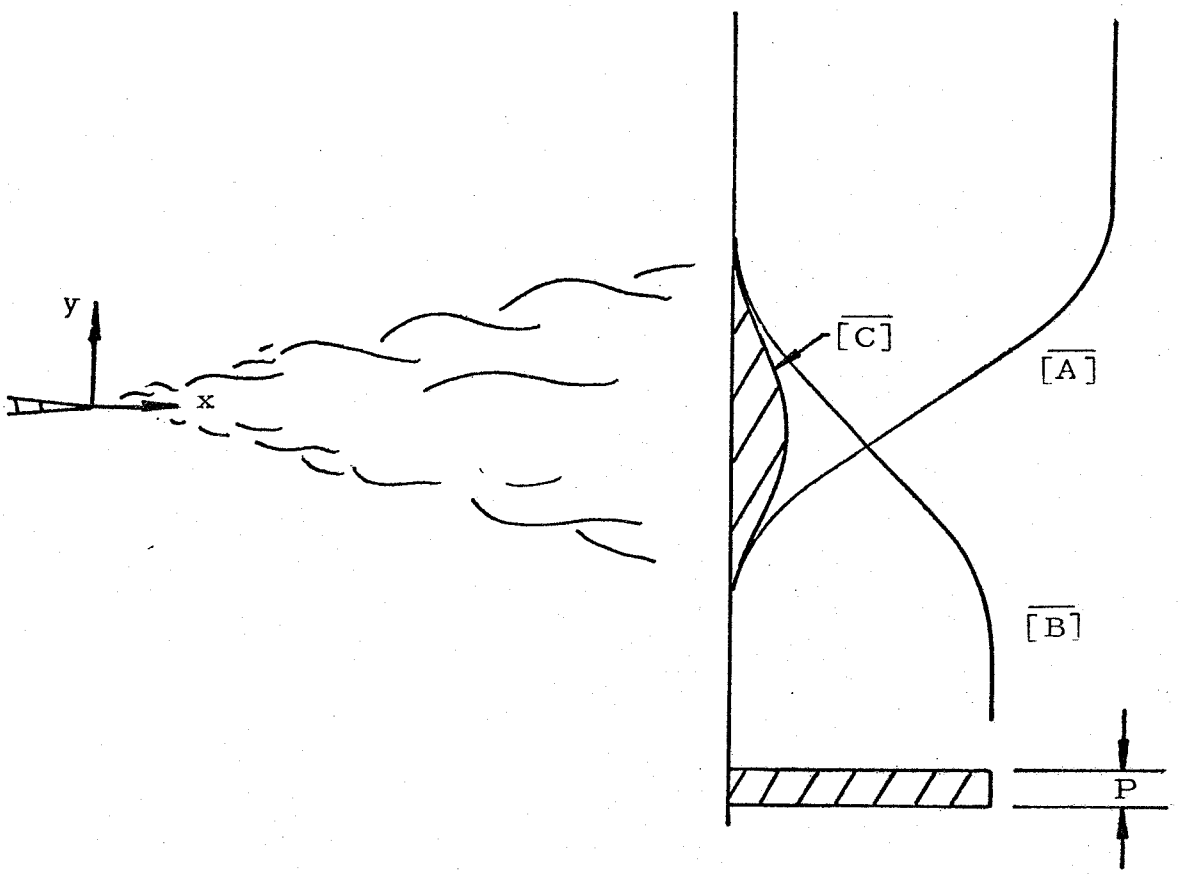

V. RESULTS AND DISCUSSION

5.1 Flow Visualization

5.1a Product Distribution

A side view of the reacting shear layer is shown in Figure 9. The lower stream is colored with an inert blue dye to label fluid that originated in that stream. The upper, high speed stream is transparent. The entrainment of the blue and clear fluids into the layer is apparent. The reaction product is red and resides in lumps associated with the large vortical structures. The photograph strongly implies that these vortices dominate both the mixing and the distribution of mixed fluid, at least at this Reynolds number.

Simultaneous plan and side views of the flow are illustrated in Figure 10. (Note that blue dye was not used for this and all subsequent photographs.) Several features of the photograph are significant. The basic two-dimensionality of the instantaneous product distribution is evident. The flow near the end walls is somewhat disturbed. When this was first observed, it was thought to be an inherent feature of the shear layer interaction with the wall. However, it is known that a secondary flow exists in the corners of the test section due to the upstream nozzle contraction. Thus, the contaminated wall region may be a result of the secondary flow. In any event, the flow near the test section centerline appears reasonably clean and basically two-dimensional, and all measurements were made there.

5.1b The Wiggle

The most interesting feature of Figure 10 is the spanwise-sinuous wiggle. Upstream of the wiggle the flow appears essentially

two-dimensional. Streamwise lines are visible downstream of the wiggle and the flow is clearly three dimensional there.

Similar streamwise streaks have been observed by shadowgraph photography in the Brown-Roshko gas apparatus for some time (Konrad 1977). They have been interpreted as streamwise vortices of alternating sign. Their origin was, however, obscure.

16 mm high speed motion pictures displayed the evolution of the sinuous vortex and the streamwise streaks, but the movie resolution was inferior to 35 mm still photographs. It is of course dangerous to infer the evolution of a flow from random snapshots, but some features of the layer are only visible in the high resolution still photographs.

Figure 11 is such a snapshot of the plan view of the layer. A wiggle has formed and another one is apparently evolving in the neighboring upstream vortex. The outer sheet of the vortex is corrugated, while the inner sheet appears relatively unperturbed. It is tempting to conclude that this is characteristic of the wiggle formation.

After the wiggle is formed, it is stretched by the global strain field of the flow. Its amplitude grows rapidly, while its wavelength remains constant. Such a stretched wiggle can be seen in Figure 11 downstream of the wiggle.

The average wavelength of the sinuous wiggle was measured from photographs to be about 1.1 times the wavelength of the initial two-dimensional Kelvin-Helmholtz waves.

A time exposure of the plan view is shown in Figure 12. The streamwise streaks represent long time averaged spanwise variations

in the mixing. The streaks first appear at the onset of the wiggle and extend to the end of the test section. The relative amplitude of the spanwise fluctuations appeared to be a maximum a short distance downstream of the wiggle location. At large Reynolds number, time exposures of the plan view indicated that the time averaged mixing along the span was moderately uniform, but streamwise streaks were still detected.

A snapshot of the plan view at large Reynolds number (Figure 13) illustrates that in spite of the introduction of three-dimensional small scale motions into the flow, the large structure is basically two-dimensional, as indicated by the product distribution.

5.2 Product Measurements

5.2a Shear Layer Time Histories

As discussed in section 2.2b, the amount of product was measured by passing a narrow beam of light through the layer. The red product attenuated the beam, and the instantaneous amount of product along the light path was measured and recorded as a function of time. Time histories of the equivalent product thickness P (Eq. 4.1) before and after the mixing transition* are shown in Figures 14a and b, respectively. Electronic noise accounts for excursions of the signal below the axis P = 0. The shear layer was about the same thickness in both runs, yet the average value of P (indicated on the vertical axis) was much higher above the transition. There were impressively large fluctuations in the instantaneous value of P even at the higher Reynolds number. Each large excursion presumably corresponds to

*Discussed in Section 5.2b.

hundred. Fortunately, the mixing in Konrad's experiment appears to approach its asymptotic value at an equivalence ratio of 10, and little change is expected for larger values of f. The physical explanation is that for a large enough equivalence ratio the amount of product formed is just limited by the entrainment of the scarce reactant into the layer, since there is an abundance of excess reactant there. Thus in Figure 16 the present work at $f \doteq 200$ can be compared with Konrad's results for $f = 10$. The most obvious feature is the rapid increase in P/δ at $Re = 5000$. At the transition P/δ jumped about 25% in the gas flow and about a factor of 7 in the aqueous layer.

Above the transition the amount of mixing is seen to be independent of Reynolds number and only a weak function of Schmidt number. The Schmidt number differed in the two cases by three orders of magnitude, yet P/δ changed by about a factor of two or less. Konrad employed the inert scalar contaminant technique which, as discussed in Section 3.1, always yields an upper bound on the actual mixing. In the present study, the chemistry is reversible, so the product measurements are a lower bound on the mixing. The finite width of the light beam also underestimates the amount of product. If the mixing is monotonic with diffusion coefficient*, then for Schmidt numbers between 0.7 and 600, P/δ must always be between the two curves. Since the gas and the water measurements are upper and lower bounds, respectively, on the mixing, it is

*This is not necessarily true. As pointed out by Prof. Philip G. Saffman, G.I. Taylor's problem of dispersion in laminar and turbulent pipe flow (Taylor, 1953 and 1954) illustrated that as the diffusion coefficient increases, the streamwise dispersion of a scalar contaminant can decrease.

a large vortex drifting through the beam. The average time interval for the passage of the large structures is indicated.

Figure 15 is a similar time history of P above the transition, but with a compressed time scale. Many large structures have passed through the beam during this record, thus giving a large statistical sample of P. Several times during this record the light beam detected almost no product, indicating that it is occasionally possible to see almost entirely through the layer even at large Re. Topologically, of course, there must always be a reaction interface and thus a finite amount of product between the two reactant fluids. However, because of high local strain rates in the turbulence this interface may locally be very thin in a high Schmidt number fluid and thus contain very little product. If the light beam only pierces through one such thin interface at some instant, then the instantaneous product thickness will be very small.

5.2b Effect of Schmidt Number

The main results of the mixing measurements for a velocity ratio of r = 0.38 are shown in Figure 16. There the (mean) equivalent product thickness P normalized by the vorticity thickness δ

$$\delta = \Delta U / \frac{\partial U}{\partial y}_{max} \qquad (5.1)$$

is plotted as a function of large scale Reynolds number $Re = \frac{\Delta U \delta}{\nu}$. Roughly speaking, P/δ represents the fraction of the layer filled with reaction product. The curve is inferred from Konrad's thesis, where a shear layer between two different gasses was studied. The highest equivalence ratio f that Konrad discussed was 10, while chemical constraints limit the present work to an equivalence ratio of a few

possible that the actual difference at high Reynolds number is considerably smaller than indicated.

Below the transition, the mixing is a strong function of Schmidt number. The gas and water measurements differ by about a factor of 12 here. If there are no flame shortening effects, the mixing should vary like $Sc^{-\frac{1}{2}}$. The observed mixing difference in the two fluids is somewhat less than this; therefore there may be flame shortening in the gaseous flow. The effect should not be too surprising. Since $Sc \doteq 1$ for the gas the local product and vorticity sheets are about the same thickness, ignoring the initial boundary layers. (As the flow is initially two-dimensioanl, no vortex amplification by stretching can occur.) If the vortex sheet radius of curvature at the vortex core is about equal to the sheet's thickness there, then the sheets are not isolated and flame shortening can occur.

Of course another possibility is experimental error associated with the aqueous measurements. P is estimated to be of the order of 500 μm at low Reynolds number. Since the mixing is so slight, modest absolute inaccuracies yield relative errors.

Bradshaw (1966) reported that the Reynolds stress in the near field of a round jet actually overshoots the final, asymptotic value for "fully developed turbulence". Roshko* suggests that the overshoot in $\overline{u'v'}$, the Reynolds stress, is due to

*Private Communication

the relatively periodic and "jitter-free" nature of the flow at the vortex sheet roll-up and for some distance downstream. Cooperative, large scale transport of momentum by the vortices is then responsible for the high correlation in velocity fluctuations, $\overline{u'v'}$. In contrast, the mixing is sensitive to the small scales and is completely independent of the Reynolds stress.

5.2c The Transition

Figure 17 illustrates the nature of the flow at the transition from a plan view of the reaction product. Immediately downstream of the splitter plate the shear layer was laminar. The vortex sheet rolled up into two-dimensional discrete vortices. At about $Re \cong 2000$, for $r = 0.38$ three-dimensional motions appeared; i.e., the "wiggle". The vorticity vector was rotated into the streamwise direction and stretched. The streamwise vortices are visible just downstream of the wiggle. The basic two-dimensional nature of the large vortices remains unaltered, however, by the small scale, three-dimensional motions.

Figure 17 clearly shows the dramatic effect of the introduction of three-dimensional motions on the amount of chemical product. Downstream of the appearance of the sinuous wiggle, P/δ increased in the transition by an order of magnitude. Konrad (1977) reported that the shear layer thickness δ was essentially unaffected by the introduction of the small scale motions.

The velocity ratio ($r \equiv \frac{U_2}{U_1}$) of the shear layer was varied to explore its influence on mixing, in particular its effect on the

transition Reynolds number and the asymptotic value of P/δ at high Re. The results are presented in Figure 18. The transition Reynolds number decreased as the velocity ratio increased. Within the accuracy of the measurements, the asymptotic value of P/δ was independent of r. This is consistent with the notion of entrainment limited mixing above the transition.

5.2d Effect of Initial Conditions

The fact that P/δ is not a unique, single-valued function of the large scale Reynolds number implies that the three-dimensional transition is influenced by the initial conditions of the laminar vortex sheet. This conclusion is not too surprising, since the shear layer is not fully three-dimensional at the wiggle and far from self similar. A further conclusion is that the onset of the three-dimensional instability (and thus the mixing transition) is not described by the large scale Reynolds number because as the flow visualization suggests (Figures 11 and 17), it is not the large structures per se that become unstable. Rather, the outer layer of the vortex sheet that has rolled up into a vortex appears to first undergo large amplitude, three-dimensional motion.

Since the mixing transition is evidently influenced by the initial conditions of the shear layer, the normalized product thickness P/δ was plotted as a function of the initial Reynolds number $\frac{U_1 \theta_1}{\nu}$ at a fixed x (Figure 19). This particular parameter was chosen because i) most of the vorticity in the initial vortex sheet originated in the boundary layer of the high speed side, and ii) most of the opposite sign vorticity from the low speed boundary

layer is quickly cancelled by diffusion of the high speed vorticity. The initial vorticity thickness θ_1 was computed as

$$\theta_1 = \left(\nu \frac{x_{eff}}{U_1}\right)^{\frac{1}{2}} \tag{5.2}$$

where x_{eff} is the effective origin of the laminar boundary layer in a zero pressure gradient. The value of x_{eff} was estimated to be 4 cm. There is considerable scatter in the data, especially at low Reynolds number and in the transition, reflecting the sensitivity of the mixing to small scale motions and the streamwise streaks in the transition. Even so, it is apparent that the transition occurs at about the same initial Reynolds number $\frac{U_1 \theta_1}{\nu}$ for velocity ratios from $r = .38$ to $r = .80$. The result lends support to the conclusion that the transition is an initial condition effect. Note that the initial parameter $\frac{x}{\theta_1}$ varied with the flow speed (Eq. 5.2). This point will be discussed in Section 5.3.

There are at least three candidates for the initial instability which results in the wiggle. The Widnall instability (Widnall, Bliss and Tsai 1974, Moore and Saffman 1975, Tsai and Widnall 1976 and Saffman 1978) was first proposed to explain circumferential waves in vortex rings and, as suggested by Saffman (1977)*, may be responsible for the wiggle in the shear layer. Briefly, the physical idea is that if a rectilinear line vortex is perturbed into a sinusoidal shape, such that the vortex is steady under its own self-induced velocity, then in the presence of an external strain field the crests of the deformed line vortex will be convected away from their unperturbed position as a consequence of the imposed strain. In

*Private communication

this way the amplitude of the sinuous perturbation grows with time.

Benney (1961) and Corcos (1978)* employed formal mathematical perturbation expansions to explore the infinitesimal three-dimensional instability. Brown (1976)* and Konrad (1977) have suggested that the Rayleigh-Taylor instability is responsible for the streamwise streaks. Their shadowgraph flow visualization did not display the wiggle, so their model does not directly incorporate it. Further work is needed to determine which, if any, of these candidates is the initial three dimensional instability in the shear layer.

5.2e Wake Mixing

The mixing in two different wake flows was briefly explored+ to compare with the shear layer behavior. A wake is formed downstream of the splitter plate when $U_1 = U_2$. Both the "regular" splitter plate and a blunt splitter plate were used. The blunt or "thick" plate had a trailing edge thickness of $d = 0.635$ cm while the regular, or thin trailing edge splitter plate was less than .003 cm thick there. The ratio of boundary layer momentum thickness θ_1 to plate thickness d at the trailing edge is small for the thick plate and large for the thin plate.

Figure 20 shows some typical time histories of the product thickness of the thick wake at $x = 8.5$ cm for four different Reynolds numbers $\frac{Ud}{\nu}$. The signal was very periodic for $\frac{Ud}{\nu} = 220$ and became less so as the Reynolds number increased. The average amount of product thickness, indicated on the vertical axis in each

*Private communication
+With the assistance of Mr. Til Liepmann

case, increased monotonically with $\frac{Ud}{\nu}$ in the transition range, as shown in Figure 21. The normalized product thickness P/δ_w is plotted as a function of the large scale wake Reynolds number $\frac{Ud}{\nu}$. The wake thickness δ_w was defined as

$$\delta_w \equiv (xd)^{\frac{1}{2}}. \tag{5.3}$$

No attempt was made to determine the precise virtual origin of the wake flow from mean velocity profiles. For the thin wake, d is taken to be $2\theta_1$. Both the thick and thin wakes exhibit a mixing transition across which the mixing jumps by an order of magnitude or more. Although there is considerable scatter in the data, it is apparent that the thick wake mixing had not reached the asymptotic value at x = 8.5 cm. The scatter for the thick plate wake is larger than might be expected from experimental error, and may reflect spanwise variations in the mixing.

Figure 22 is another plot of the wake data, but with the initial boundary layer Reynolds number $\frac{U_1\theta_1}{\nu}$ as the abscissa. In contrast to Figure 21, the thin plate wake now transitions at a higher Reynolds number, as might be expected. Note that these coordinates for the wake are the same as in Figure 19 for the shear layer.

A direct comparison of the thin wake and shear layer is presented in Figure 23. The two flows exhibit a transition in the mixing at the same initial boundary layer Reynolds number $\frac{U_1\theta_1}{\nu}$. Since the definitions of δ and δ_w (Eqs. 5.1 and 5.3, respectively) are arbitrary, there is no reason to expect the asymptotic values of

parameter $T \sim \frac{Sc}{Re^{\frac{1}{2}}}$ predicts that if Sc is high enough, then there will be a large Re at which the mixing undergoes a transition even if the flow is already three-dimensional and full of small scale motions. The aqueous Schmidt number is only about 600 and the Reynolds number at which the model predicts a mixing transition ($T \sim 1$) roughly corresponds to a transition in the flow itself $\left(\frac{Sc}{Re^{\frac{1}{2}}} \sim \frac{600}{(10^4)^{\frac{1}{2}}} \sim 6\right)$, i.e., the introduction of three-dimensional motions. In this respect the mixing in a fluid with $Sc \sim 10^6$ or larger would be useful as a test of the model where the flow is self-similar, but then Re would have to be 10^{12}!

5.3 Speculations

The mixing transition was found to be a non-unique function of the large-scale Reynolds number $\frac{\Delta U \delta}{\nu}$ (Fig. 15) and may be completely independent of it. The transition appears to be largely independent of the velocity ratio when plotted as a function of $\frac{U_1 \theta_1}{\nu}$ at a fixed downstream station x. If the large scale Reynolds number and velocity ratio are unimportant in determing the transition, then it is possible that only the initial high speed vortex sheet Reynolds number $\frac{U_1 \theta_1}{\nu}$ and normalized distance x/θ_1 are important in defining the transition.

Note that in Figure 23 there appears to be a trend for the shear layer to transition at a slightly higher initial Reynolds number $\frac{U_1 \theta_1}{\nu}$ as the velocity ratio increases. A possible explanation is that there is an indirect effect of velocity ratio on the transition through the initial boundary layers. For example, a prerequisite for transition may be that the bulk of the low speed vorticity is cancelled by viscous diffusion of high speed vorticity. In this event the

effective thickness of the vortex sheet would be more like $(\theta_1 + \theta_2)$ rather than simply θ_1, at least for velocity ratios bounded away from $r = 0$. As $r \to 0$, the ratio $\frac{\theta_2}{\theta_1}$ increases without limit for a symmetric contraction, yet the flux of low speed vorticity leaving the splitter plate is quite low compared to the high speed vorticity flux. No attempt was made here to substitute more appropriate initial conditions for $\frac{U_1\theta_1}{\nu}$ and $\frac{x}{\theta_1}$, but the possibility for improvement remains.

A speculative relationship between these two parameters and the normalized product P/δ is sketched in Figure 24a. At large $\frac{U_1\theta_1}{\nu}$ and $\frac{x}{\theta_1}$, P/δ is large while near the origin P/δ is small. P/δ must remain small for all $\frac{U_1\theta_1}{\nu}$ provided $\frac{x}{\theta_1} \tilde{=} 0$. Near the other coordinate axis, P/δ is small as $\frac{x}{\theta_1}$ increases since $\frac{U_1\theta_1}{\nu}$ is so low that the initial laminar flow is stable to even two-dimensional perturbations (e.g., if $\frac{U_1\theta_1}{\nu} < 20$, a wake remains laminar). Note that a laminar shear layer will eventually become unstable no matter how low the initial Reynolds number $\frac{U_1\theta_1}{\nu}$ is, because the laminar layer grows slowly until the local Re, $\frac{\Delta U\delta}{\nu} > Re_{CRIT}$. Thus the shear layer will not behave precisely as the sketch suggests in the limit of $\frac{U_1\theta_1}{\nu} \to 0$ and $\frac{x}{\theta_1} \to \infty$.

Because of little mixing (and thus measurement accuracy) near the splitter plate and end wall contamination effects downstream, the measurement station x was held essentially constant. Both $\frac{x}{\theta_1}$ and $\frac{U_1\theta_1}{\nu}$ were varied by changes in flow speed and both go like $U_1^{\frac{1}{2}}$. Thus, the actual trace of the data presented in Figure 18 is not parallel to the $\frac{U_1\theta_1}{\nu}$ axis at a constant $\frac{x}{\theta_1}$ but rather

along a diagonal as illustrated in Figure 22b. It represents a composite of the influence of the two independent variables. The multiplicative product of these two variables $\frac{U_1 x_1}{\nu}$ is a quantity that Bradshaw (1966) found in a near jet flow ($r = 0$) to roughly define the shear layer transition length largely independent of θ_1 for $500 < \frac{U_1 \theta_1}{\nu} < 1000$. Curves of constant $\frac{U_1 x}{\nu}$ are hyperbolas in the $\frac{U_1 \theta_1}{\nu} - \frac{x}{\theta_1}$ plane and are more or less orthogonal to the aforementioned diagonal trace along which the present measurements were made. Assuming that Bradshaw's observation is approximately true over a large range of $\frac{U_1 \theta_1}{\nu}$, the contours of constant P/δ may be approximated by the hyperbolas $\frac{U_1 x}{\nu}$ = constant in Figure 24b.

The downstream station for fully developed turbulence is

$$x = 162\,\theta_1 + 4 \times 10^5 \frac{\nu}{U_1} \quad \text{for} \quad 500 < \frac{U_1 \theta_1}{\nu} < 1000$$

according to Bradshaw's hot wire measurements for $r = 0$. The aqueous mixing achieves its asymptotic value at about $x = 162\,\theta_1 + 2.5 \times 10^5 \frac{\nu}{U_1}$ for the conditions tested. In light of Broadwell's model, agreement between the mixing transition and velocity measurements on the exact location of fully developed turbulence is not to be expected, since the mixing will reach its entrainment-limited asymptotic value as soon as enough small scales have formed to mix the reactants at the rate they are being entrained. The velocity field need not be perfectly self-similar there.

As the flow speed of the Bradshaw jet was doubled, while maintaining a laminar boundary layer, he observed that the station of fully-developed turbulence moved upstream by almost a factor of

two. When θ_1 was increased with a longer jet nozzle at a fixed U_1, the station moved downstream only slightly. These two results are consistent with the sketches of Figures 24a and b, and imply that the approach to fully developed turbulence does not scale with the initial momentum thickness θ_1. Bradshaw's contrary comment, while approximately correct for a limited range of test conditions, must not be generally valid if the present speculations are embraced.

It is possible that there are two limiting cases for transition: very low initial Reynolds number and very high. The shear layer vortex sheet is unstable to two-dimensional Kelvin-Helmholtz waves for $\frac{U_1 \theta_1}{\nu} \gtrsim 10$. If $\frac{U_1 \theta_1}{\nu}$ is less than some critical number of order 100, then the roll-up is apparently stable to three-dimensional perturbations. In the shear layer the flow must somehow become turbulent far downstream since the large scale Reynolds number increases with x. The transition process to three-dimensional, turbulent flow may be different in this case than in the other extreme of high initial Reynolds number, where the plan view photographs indicate that the three-dimensional instability occurs during the vortex sheet roll-up, producing the "wiggle". Significantly, at low $\frac{U_1 \theta_1}{\nu}$ the wiggle was not observed even though the flow appeared to develop three-dimensional motions.

The second general idea suggested here is that the three-dimensional transition in the shear layer is very much like that in the wake layer. Certainly the two dimensional transition, i.e., laminar to non-steady, two-dimensional motion, has many common features in the two flows. In both cases the plane, laminar vortex

sheet becomes unstable to two dimensional perturbations and rolls up into discrete vortices. In the wake (r = 1) the vortices are of opposite sign, while for the r = 0 shear layer they are of like sign*.

The critical Reynolds number $\frac{U_1 \theta_1}{\nu}$ for the wake to roll up into two-dimensional vortices must, however, be somewhat higher than for the r = 0 shear layer because of two effects. Vorticity diffusion causes cancellation of opposite-signal vorticity in the wake vortex sheet, reducing the vorticity magnitude as the Reynolds number decreases. In the r = 0 shear layer there is only one sign of vorticity present, so there can be no cancellation. The second effect is also due to the presence of the opposite signed vorticity in the wake. Imagine that every fluid element containing vorticity in the wake is arbitrarily paired to a nearby element containing exactly the same amount of opposite-signed vorticity. The pair of elemental vortices behaves like a dipole at distances that are large compared to the separation of the elements, in contrast to the much stronger monopole character of an unpaired vortical element. This is an inviscid kind of cancellation of the long range effects of the opposite signed vorticity. The induced velocities of the wake are in this sense somewhat weaker than for the corresponding shear layer, and the laminar flow is correspondingly more stable at the same $\frac{U_1 \theta_1}{\nu}$.

The thin wake and shear layer are influenced by two independent initial condition parameters, $\frac{x}{\theta_1}$ and $\frac{U_1 \theta_1}{\nu}$. The thick wake introduces another parameter, the ratio of the boundary layer thick-

*An interesting question is what is the lowest value of r for which vortices of opposite sign are shed from the thin plate. They have been observed for r = 0.8, for example.

ness to the plate thickness $\frac{\theta_1}{d}$. Since the separated boundary layers off of the thick splitter plate are initially far apart and thus each subject to the Kelvin-Helmholtz instability whereas the thin plate unites the two boundary layers together immediately, it is possible that the thick plate may exhibit additional frequency locking effects compared to the thin plate flow for the case of $r < 1$. Such

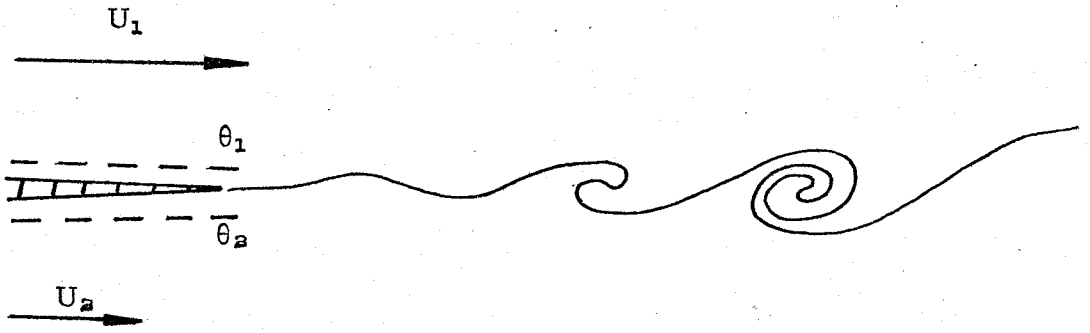

THIN PLATE SHEAR LAYER, $\frac{\theta_1}{d} >> 1$.

THICK PLATE SHEAR LAYER, $\frac{\theta_1}{d} << 1$.

interactions of the Kelvin-Helmholtz and wake modes were proposed by Roshko and Fiszdon (1969) to influence the near wake flow. However, due to the sensitivity of the far field shear layer to initial perturbations, it is reasonable to suggest that the far field shear layer may be quite sensitive to perturbations introduced by the self-oscillating near field base flow. Like a chameleon, the separated boundary layer first behaves like a shear layer, then in the larger sense like a wake, and finally reverts back into a shear layer far downstream. By tuning the base flow oscillator it may be possible to control the mixing in the far field shear layer. The interesting features of a shear layer with a built-in self-oscillator remain to be explored.

VI. CONCLUSIONS

The amount of molecular scale mixing in an aqueous shear layer ($Sc \doteq 600$) was measured using a chemical reaction technique. The results were compared with Konrad's gaseous mixing measurements ($Sc \doteq 0.7$). At low Reynolds number, the effect of Schmidt number on the mixing was pronounced, while at high Reynolds number, the mixing differed by roughly a factor of two or less. Thus a three order of magnitude variation in Schmidt number produced only a relatively weak change in mixing at large Re. Above the transition, the mixing was independent of Re. This was consistent with qualitative predictions of Broadwell's mixing model. A transition region for the mixing, first observed by Konrad in a gas flow, was again found to correspond to the introduction of small-scale, three-dimensional motions into the layer. The aqueous mixing was very sensitive to the presence of these small scales. The large-structure transition Reynolds number was found to vary with velocity ratio, implying that the instability is dependent on initial conditions. The important parameters are suggested to be the initial vortex sheet thickness and Reynolds number.

The unique flow visualization provided by the chemistry revealed a spanwise-sinuous "wiggle" which is believed to play an important role in introducing streamwise vortices and small scale motions in the mixing layer. The initial instability which generates the wiggle is not yet known, although several candidates exist.

Further work is necessary to determine the nature of the initial three-dimensional instability. The precise evolution of the wiggle

and its effect on spanwise variations of the mixing in the mixing layer remain uncertain.

APPENDIX A

An Estimate of the Mixing Interface Thickness at Large Schmidt Number

In a turbulent flow, the mixing interface is thinned by the turbulent strain field. For fluids with $S_c \gg 1$, the interface is assumed to be thin compared to the Kolmogorov microscale, λ_o. This is in agreement with theoretical predictions of Batchelor (1959), and experimental results of Gibson and Schwarz (1963). A thin interface will locally be subjected to strain rates as large as the microscale strain rate σ_o. This strain rate is just the reciprocal of the characteristic vorticity diffusion time across the microscale.

$$\sigma_o \sim \left(\frac{\lambda_o^2}{\nu}\right)^{-1}$$

The microscale goes like $\lambda_o \sim \delta Re^{-\frac{3}{4}}$ (Landau and Lifshitz, 1959) so that

$$\sigma_o \sim \frac{\nu}{\delta^2} Re^{3/2}. \qquad (A.1)$$

If a diffusion interface of zero thickness at $t = 0$ is subjected to plain strain at a constant rate σ, the interface thickness ξ evolves as sketched below.

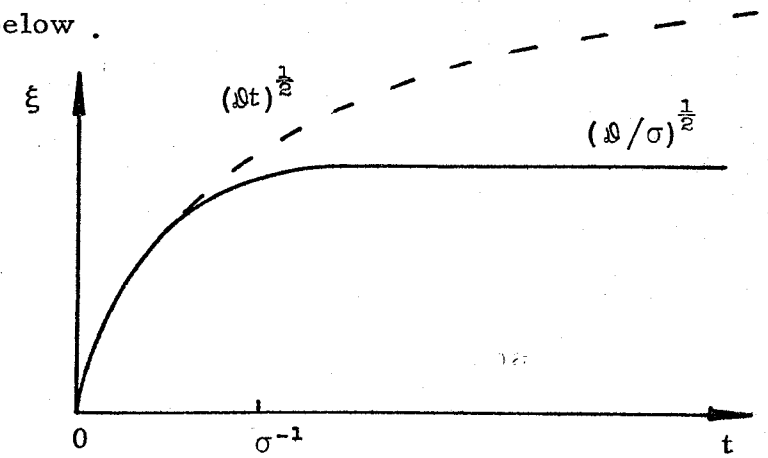

For $t \ll \sigma^{-1}$, the thickness increases like $(\mathcal{D}t)^{\frac{1}{2}}$. When $t \gg \sigma^{-1}$, ξ asymptotes to a value

$$\xi \sim (\mathcal{D}/\sigma)^{\frac{1}{2}} \tag{A.2}$$

independent of time. Combining A.1 and A.2 yields

$$\xi \sim S_c^{-\frac{1}{2}} Re^{-\frac{3}{4}} \delta . \tag{A.3}$$

Typical flow conditions in the water tunnel are $S_c \sim 500$, $Re \sim 10^4$, and $\delta = 1$cm, so that A.3 yields

$$\xi \sim 3 \times 10^{-5} \text{ cm}$$

which is less than the wavelength of light.

This is only a very rough estimate since the Kolmogorov expressions are derived from dimensional arguments. Also, the interface is not necessarily always this thin. Obviously once mixing has been achieved in a large region the interface is much thicker. This is an estimate of the thinnest interfaces expected in the turbulence.

APPENDIX B

The Laminar Reacting Shear Layer

The solution to the laminar, reacting shear layer is derived, using a boundary layer approximation. Streamwise gradients and the initial splitter plate boundary layers are neglected. Thus the temporal problem is actually solved, and the solution is then applied to the spatial flow with the aforementioned approximations.

Vorticity

The vorticity equation for 2-D, uniform density flow with conservative forces is

$$\frac{D\underline{\omega}}{D_t} = \nu\nabla^2\underline{\omega}\,, \qquad \underline{\omega} = \omega(y, t)\,(\text{unit z vector}) \quad \text{(B. 1)}$$

the Eulerian heat equation. The initial vorticity distribution is taken to be a delta function, or infinitely thin gaussian. The solution to equation (B. 1) is a gaussian for all $t > 0$,

$$\omega = \frac{\text{const.}}{(\pi\nu t)^{\frac{1}{2}}}\, e^{\frac{-y^2}{\nu t}}\,.$$

Now the total amount of vorticity integrated through the vortex sheet is just the velocity jump, Δu, across the sheet.

$$\int_{-\infty}^{\infty} \omega(y, t)dy = \Delta u$$

Therefore (B. 2)

$$\omega(y, t) = \frac{\Delta u}{(\pi\nu t)^{\frac{1}{2}}}\, e^{\frac{-y^2}{\nu t}}\,.$$

and

$$\delta \equiv \int_{-\infty}^{\infty} \frac{\omega}{\omega_{max}} dy = \frac{\Delta u}{\omega_{max}} = (\pi \nu t)^{\frac{1}{2}} . \qquad (B.3)$$

Product *

Dilute reactants imply that there is no effect of the chemistry on the flow. Thus the product distribution is independent of the vorticity field in the temporal, laminar problem. Assuming fast, irreversible chemistry, the problem remarkably enough, is independent of chemistry. The reactants satisfy the familiar diffusion, or heat, equation

$$\frac{D}{Dt} K_A = \mathcal{D} \nabla^2 K_A$$

$$\frac{D}{Dt} K_B = \mathcal{D} \nabla^2 K_B \qquad (B.4)$$

where, for simplicity, all diffusion coefficients are assumed equal. Here K_A and K_B are the molar concentrations of reactants A and B, normalized by their respective freestream values, e.g.,

$$K_A = \frac{[A]}{[A]_\infty} .$$

If the chemistry is fast enough, the two reactants cannot coexist macroscopically. Thus the reaction occurs within a thin sheet whose thickness is determined by molecular scales (e.g., in a gas, a few mean free paths). Idealizing this sheet as an infinitely thin reaction surface, boundary conditions for equation B.3 are

$$\begin{aligned} K_A = K_B &= 0 \quad \text{at the reaction surface} \\ K_A = K_B &= 1 \quad \text{in the freestream,} \quad y \to \pm \infty \end{aligned} \qquad (B.5)$$

*This section paraphrases some classroom lectures of Prof. F. E. Marble.

The reaction is second order, with stoichiometric ratio f*.

$$A + f^* B \rightarrow f^* C \qquad (B.6)$$

Thus, at the reaction surface the flux of reactant B must exceed that of A by the factor f*.

$$\left(\frac{\nabla[B]}{\nabla[A]}\right)_{\text{Reaction surface}} = f^*$$

or

$$\frac{[B]_\infty}{[A]_\infty}\left(\frac{\nabla K_B}{\nabla K_A}\right)_{\text{Reaction surface}} = f^*.$$

Define the equivalence ratio

$$f \equiv \frac{[A]_\infty}{[B]_\infty} f^*.$$

Then

$$\left(\frac{\nabla K_B}{\nabla K_A}\right)_{\text{Reaction surface}} = f \ . \qquad (B.7)$$

At t = 0, the reactant distributions are step functions. The solution to the heat equations B.4 for an initial step function is just the error function. The boundary conditions B.5 and B.6 imply that

$$K_A(\eta) = \frac{\operatorname{erf}\left(\frac{\eta}{2} - \alpha\right) + \operatorname{erf}\alpha}{1 + \operatorname{erf}\alpha}$$

and

$$K_B(\eta) = \frac{\operatorname{erf}\left(-\frac{\eta}{2} + \alpha\right) - \operatorname{erf}\alpha}{1 - \operatorname{erf}\alpha}$$

where η is the similarity variable

$$\eta = \frac{y}{(\mathcal{D}t)^{\frac{1}{2}}}$$

and

$$\operatorname{erf}\alpha = \frac{1-f}{1+f} \ .$$

Note that for the symmetric case of $f = 1$, $\operatorname{erf}\alpha = 0$ and $\alpha = 0$. Thus

$$K_A(\eta) = \operatorname{erf}\frac{\eta}{2} = K_B(-\eta).$$

The reaction product also satisfies the Eulerian heat equation everywhere except at the reaction surface.

$$\frac{D}{Dt}K_C = \mathcal{D}\nabla^2 K_C \ , \qquad K_C \equiv \frac{[C]}{[C]_{max}} \tag{B.8}$$

Product is formed only at the reaction surface and diffuses away down concentration gradients. The characteristic diffusion length of product into each reactant is equal to the diffusion length of the reactant since all diffusion coefficients are assumed equal. The total amount of product formed must be equal to the total amount of reactant B consumed from equation B.5. Thus, the solution of equation B.8 is

$$K_C = \begin{cases} 1 - K_A(\eta) & \eta \geq 0 \\ \\ 1 - K_B(\eta) & \eta \leq 0 \ . \end{cases} \tag{B.9}$$

The maximum concentration of product, $[C]_{max}$, occurs at the reaction surface. Its value can be determined from the fact that since the reaction surface has zero thickness in the macroscopic view, it has no volume and thus no storage capability. The diffusive flux of reactant into the surface therefore must equal the flux of product away from the surface, even in this nonsteady case.

$$\mathcal{D}\frac{\partial}{\partial y}\left(-[C]_+ + [C]_-\right) = \mathcal{D}\frac{\partial}{\partial y}[B]$$

$$\frac{\partial}{\partial y}\left(-K_{C_+} + K_{C_-}\right) = \frac{[B]_{max}}{[C]_{max}} \frac{\partial K_B}{\partial y}$$

B. 8 implies

$$\frac{\partial K_A}{\partial y} + \frac{\partial K_B}{\partial y} = \frac{[B]_{max}}{[C]_{max}} \frac{\partial K_B}{\partial y}$$

$$\frac{\partial K_A}{\partial y} = \left(\frac{[B]_{max}}{[C]_{max}} - 1\right) \frac{\partial K_B}{\partial y}$$

$$\frac{1}{1 + \operatorname{erf}\alpha} = \left(\frac{[B]_{max}}{[C]_{max}} - 1\right) \frac{1}{1 - \operatorname{erf}\alpha}$$

therefore

$$[C]_{max} = \frac{1 + \operatorname{erf}\alpha}{2} [B]_{max}$$

independent of time. The product thickness is defined as

$$P \equiv \int \frac{[C]}{[B]_{max}} dy \ .$$

It is the total amount of product formed (or reactant B consumed) normalized by the freestream concentration of reactant B. The consumption rate of reactant B is

$$\mathcal{D}[B]_{max} \nabla K_B = [B]_\infty \left(\frac{\mathcal{D}}{\pi t}\right)^{\frac{1}{2}} \frac{e^{-\alpha^2}}{1 - \operatorname{erf}\alpha} \ .$$

The total amount of B consumed is

$$[B]_\infty \int_0^t \left(\frac{\mathcal{D}}{\pi t}\right)^{\frac{1}{2}} \frac{e^{-\alpha^2}}{1 - \operatorname{erf}\alpha} dt = 2[B]_\infty \left(\frac{\mathcal{D}t}{\pi}\right)^{\frac{1}{2}} \frac{e^{-\alpha^2}}{1 - \operatorname{erf}\alpha} \ .$$

Therefore

$$P = \tfrac{1}{2}\left(\frac{\mathcal{D}t}{\pi}\right)^{\frac{1}{2}} \frac{e^{-\alpha^2}}{1 - \operatorname{erf}\alpha} \cdot$$

The ratio of product to vorticity thickness is

$$\frac{P}{\delta} = \frac{2}{\pi} \frac{e^{-\alpha^2}}{1 - \operatorname{erf}\alpha} Sc^{\frac{1}{2}} \cdot \qquad \text{(B.10)}$$

(Note, if $P \equiv \int_{-\infty}^{\infty} \frac{[C]}{[C]_{max}} dy$ in the same manner as the vorticity thickness (Eq. B.3) then $\frac{P}{\delta} = \frac{4}{\pi} \frac{e^{-\alpha^2}}{(1 - \operatorname{erf}\alpha)(1 + \operatorname{erf}\alpha)} Sc^{\frac{1}{2}}$)

P/δ is independent of time. Thus if the interface is strained in the direction normal to the vorticity vector so that no vortex stretching occurs, then P/δ is independent of stretching also. Further, as long as the radius of curvature of the interface is large compared to its thickness, the curved interface can be approximated as plane and this solution (Eq. B. 10) is appropriate.

APPENDIX C

Details of the Phenolphthalein Reaction

Since the ideal reaction is irreversible (see Section 3.3), it was desirable to minimize the degree to which the red product disappeared in the reversible phenolphthalein reaction. The approach was to operate at a large equivalence ratio, i.e., an excess of $[OH]^-$ reactant, so that an isolated reaction surface tended to move toward the phenolphthalein reactant (see Appendix B). Now the chemical product in a fast reaction is always produced at the reaction surface and diffuses away down concentration gradients. Roughly speaking, the freestream excess of $(OH)^-$ caused the reaction surface to retreat into the phenolphthalein reactant, leaving behind the bulk of the red reaction product. Because this "orphaned" product found itself in a region of ever increasing pH, it tended to remain as red reaction product, reflecting the chemical equilibrium of its environment. Only the small fraction of the red product which diffused toward the phenolphthalein reactant found itself in a low pH environment and thus reverted back into its reactants. Of course, this reverse reaction locally releases $(OH)^-$ reactant, altering its concentration profile. For the plane reaction surface at an equivalence ratio of 10^{-2} an estimate of the fraction of red product which was "lost" was obtained by graphical means to be about 10% for $pH_\infty = 12$ and perhaps 40% for $pH_\infty = 11$.

A difficulty associated with the phenolphthalein reaction is the unfortunate tendency of the red product to disappear due to a secondary reaction as the local pH increases above 11.5. Thus a compromise

freestream value of pH ≐ 11.7 was selected to minimize the secondary reaction while still "tricking" the bulk of the red reaction product to remain red.

References

Batchelor, G.K. 1959 "Small scale variation of convected quantities like temperature in a turbulent fluid, Part 1.", J. Fluid Mech. 5, 113.

Benney, D.J. 1961 "A non-linear theory for oscillations in a parallel flow", J. Fluid Mech. 10, 209.

Bradshaw, P. 1966 "The effect of initial conditions on the development of a free shear layer", J. Fluid Mech. 26, 225.

Brown, G.L. and Dimotakis, P.E. 1976 "The mixing layer at high Reynolds number large structure dynamics and entrainment", J. Fluid Mech. 78, 535.

Brown, G.L. and Roshko, A. 1974 "On density effects and large structure in turbulent mixing layers", J. Fluid Mech. 64, 775.

Caldin, E.F. 1964 Fast reactions in solution, Wiley, pp. 66 - 67.

Czerlinski, G. and Eigen, M. 1959 "Eine Temperatursprungmethode zur untersuchung schischer relaxation", Zeitschrift fur Electrochemie BD, 63, NR 6, 652.

Gibson, C.H. and Schwarz, W.H. 1963 "The universal equilibrium spectra of turbulent velocity and scalar fields", J. Fluid Mech. 16, 365.

Gluck, D.F., Gille, J.P., Simkin, D.J. and Zukoski, E.E. 1966 "Distortion of the liquid surface during tank discharge under low G conditions", Aerospace Chemical Engineering, Chemical Engineering Progress Symposium Series, 62, no. 61, 150.

Kolthoff, I.M. 1937 Acid-Base Indicators, MacMillan, 221.

Konrad, J.H. 1977 "An experimental investigation of mixing in two-dimensional turbulent shear flows with applications to diffusion-limited chemical reactions", Ph.D. Thesis, California Institute of Technology, 1977 and Project SQUID Technical Report CIT-8-PU, December 1976.

Landau, L.D. and Lifshitz, E.M. 1959 Fluid Mechanics, Pergamon Press, 122.

Marble, F.E. and Broadwell, J.E. 1977 "The coherent flame model for turbulent chemical reactions", TRW Report, 29314-6001-RE-00.

Moore, D.W. and Saffman, P.G. 1975 "The instability of a straight vortex filament in a strain field", J. Fluid Mech. 346, 413.

Roshko, A. and Fiszdon, W. 1969 "On the persistence of transition in the near wake!", in Problems of Hydrodynamics and Continuum Mechanics published by Soc. for Indust. and Appl. Math., Philadelphia, 606-616.

Saffman, P.G. 1978 "The number of waves on unstable vortex rings", J. Fluid Mech. 84, 625.

Taylor, G.I. 1953 "Dispersion of soluble matter in solvent flowing slowly through a tube", Proceedings of the Royal Society of America, 219, 186.

Taylor, G.I. 1954 "The dispersion of matter in turbulent flow through a pipe", Proceedings of the Royal Society of America, CCXXIII, 446.

Tennekes, H. and Lumley, J.L. 1972 A First Course in Turbulence, MIT Press, 279.

Toor, H.L. March 1962 "Mass transfer in dilute turbulent and non-turbulent systems with rapid irreversible reactions and equal diffusivities", A.I.Ch.E. Journal 8, No. 1, 70.

Tsai, C-Y and Widnall, S.E. 1976 "The stability of short waves on a straight vortex filament in a weak externally imposed strain field", J. Fluid Mech. 73, 721.

Weddell, D. 1941 "Turbulent mixing in gas flames", Ph.D. Thesis, Massachusetts Institute of Technology, 115.

Widnall, S.E., Bliss, D.B., and Tsai, C.Y. 1974 "The instability of short waves on a vortex ring", J. Fluid Mech. 66, 35.

Witte, A.B., Broadwell, J.E., Shackleford, W.L., Cummings, J.C., Trost, J.E., Whiteman, A.S., Marble, F.E., Crawford, D.R. and Jacobs, T.A. 1974 "Aerodynamic reactive flow studies of the H_2F_2 laser-II", Air Force Weapons Lab, Kirtland Air Force Base, New Mexico, AFWL-TE-74-78, 33.

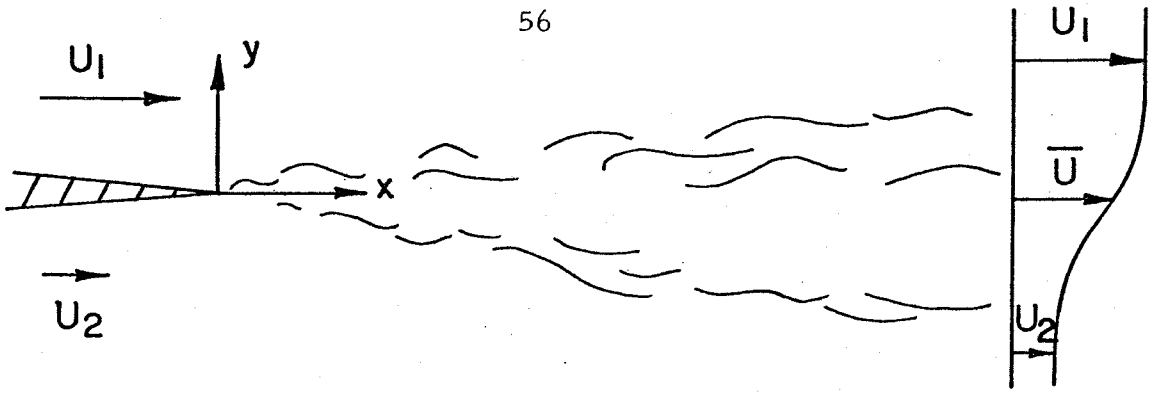

FIG. 1 FLOW GEOMETRY

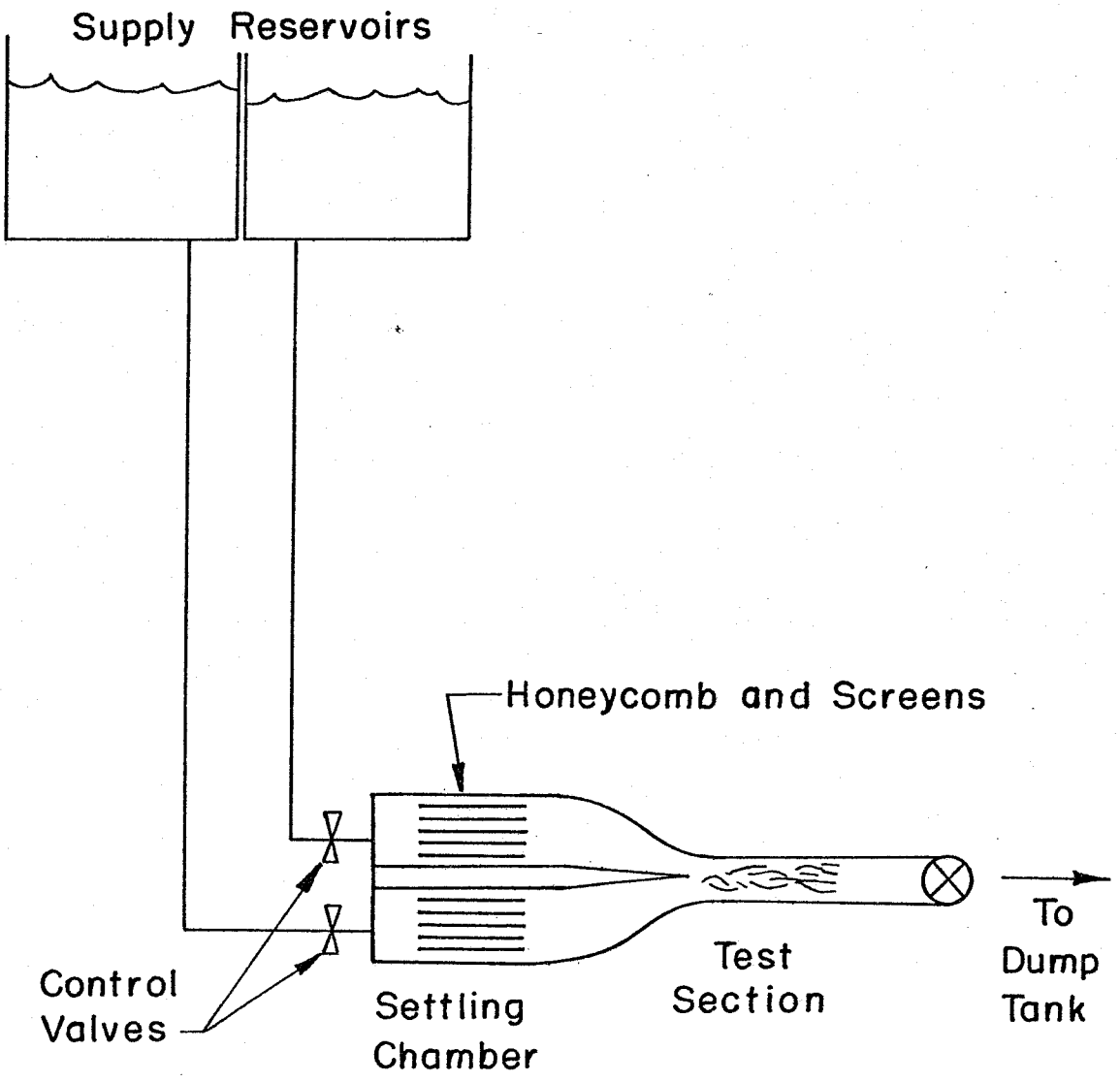

FIG. 2 APPARATUS SCHEMATIC

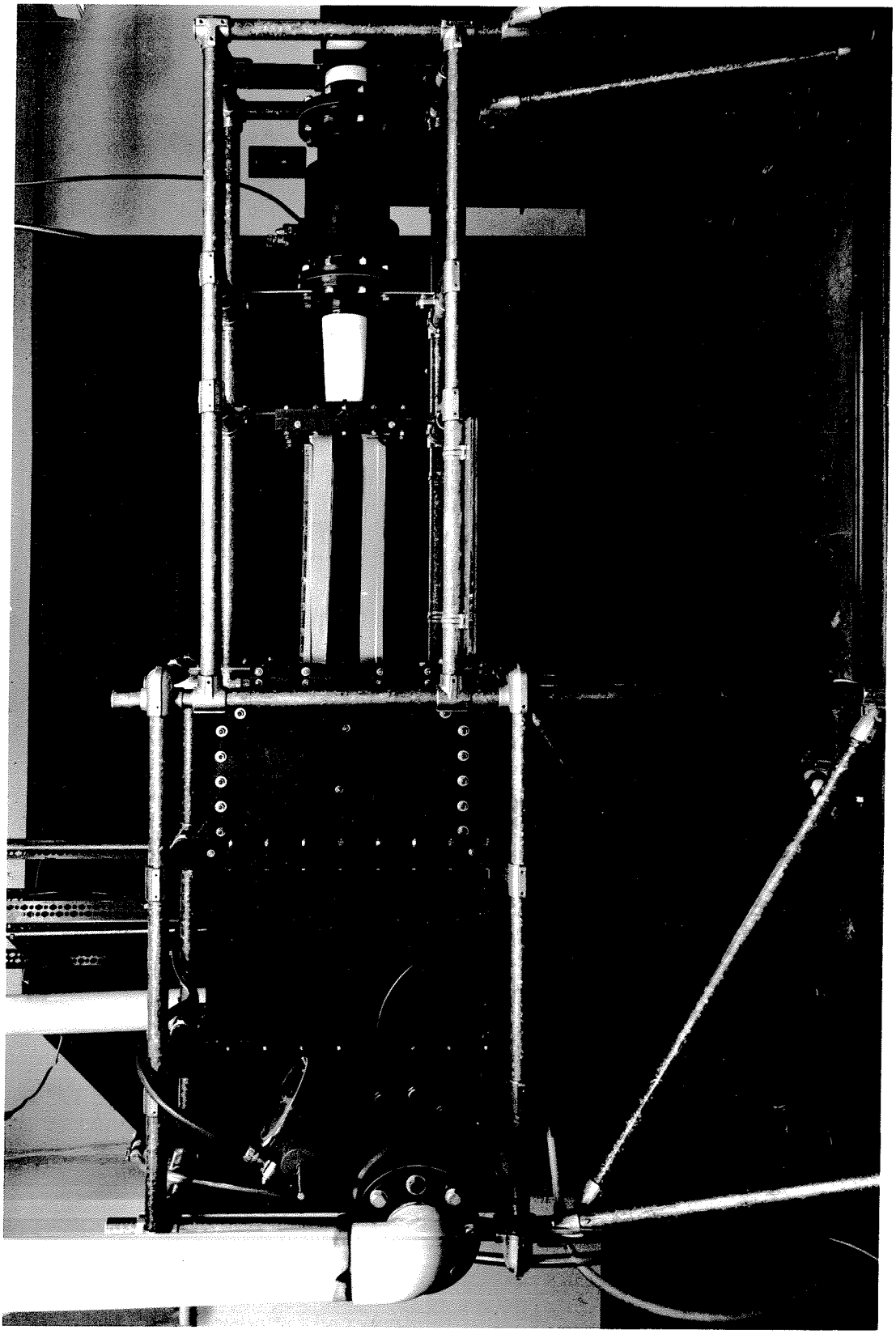

FIG. 3 PHOTOGRAPH OF APPARATUS

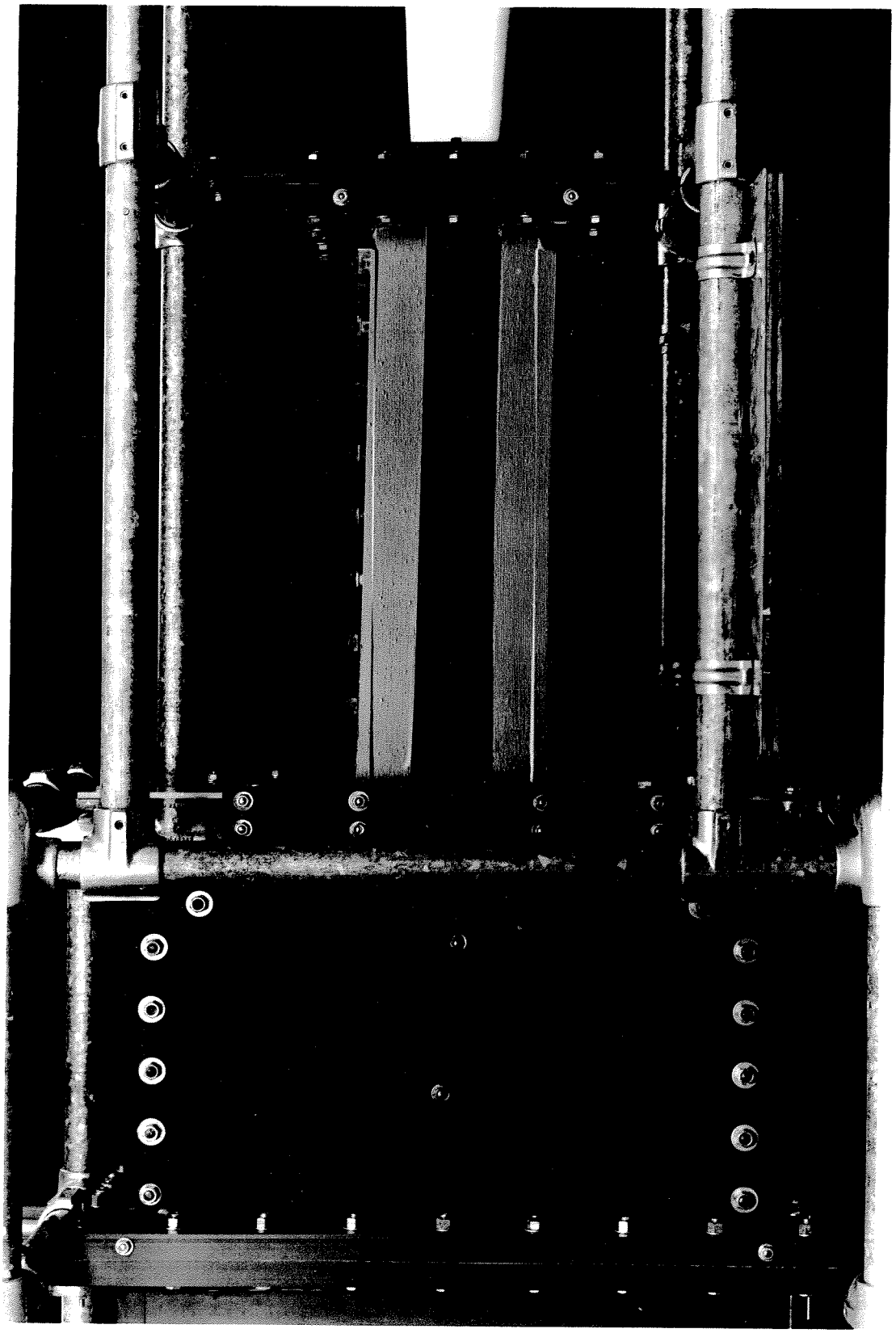

FIG. 4 CLOSE UP OF TEST SECTION AND CONTRACTION

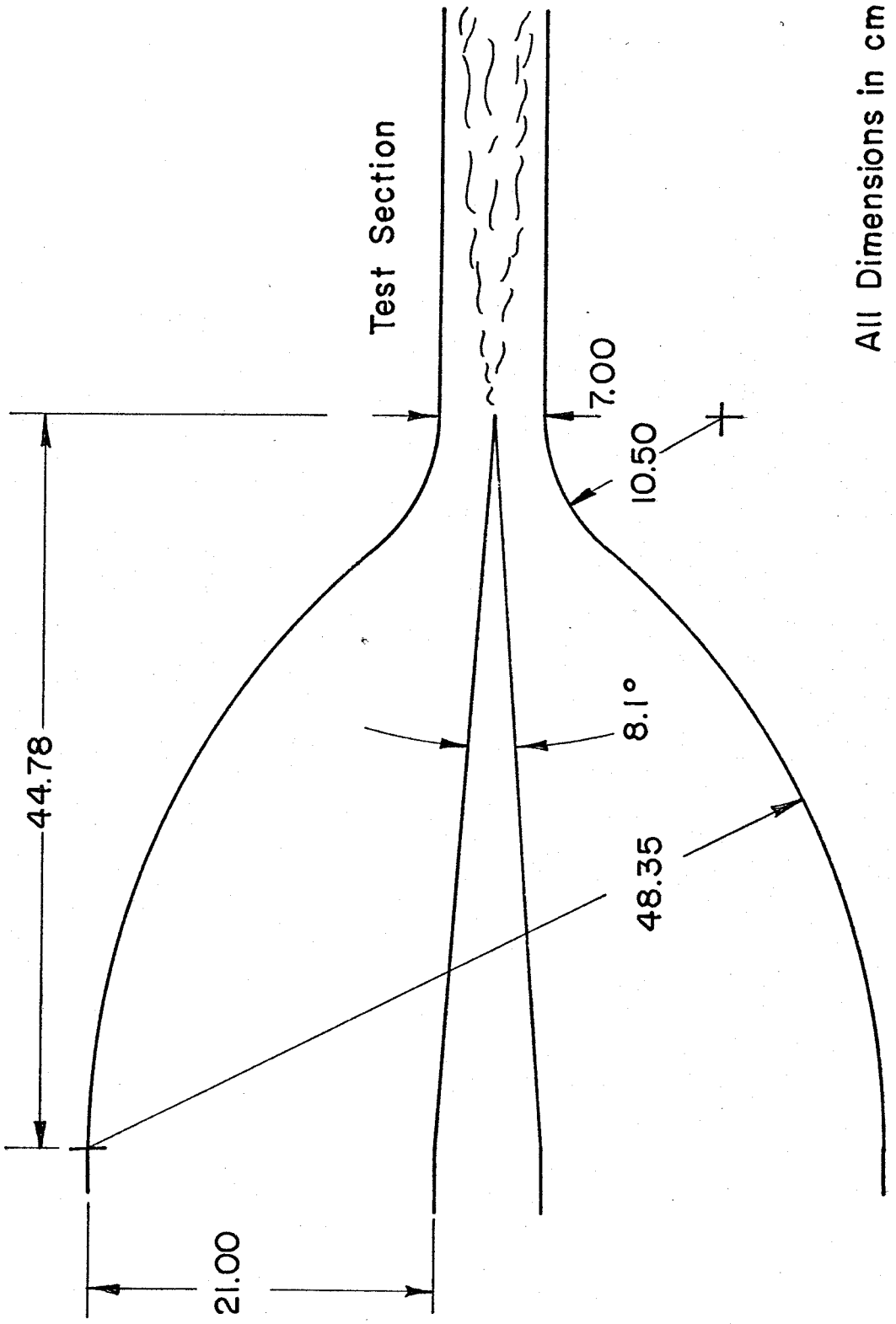

FIG. 5 CONTRACTION DIMENSIONS

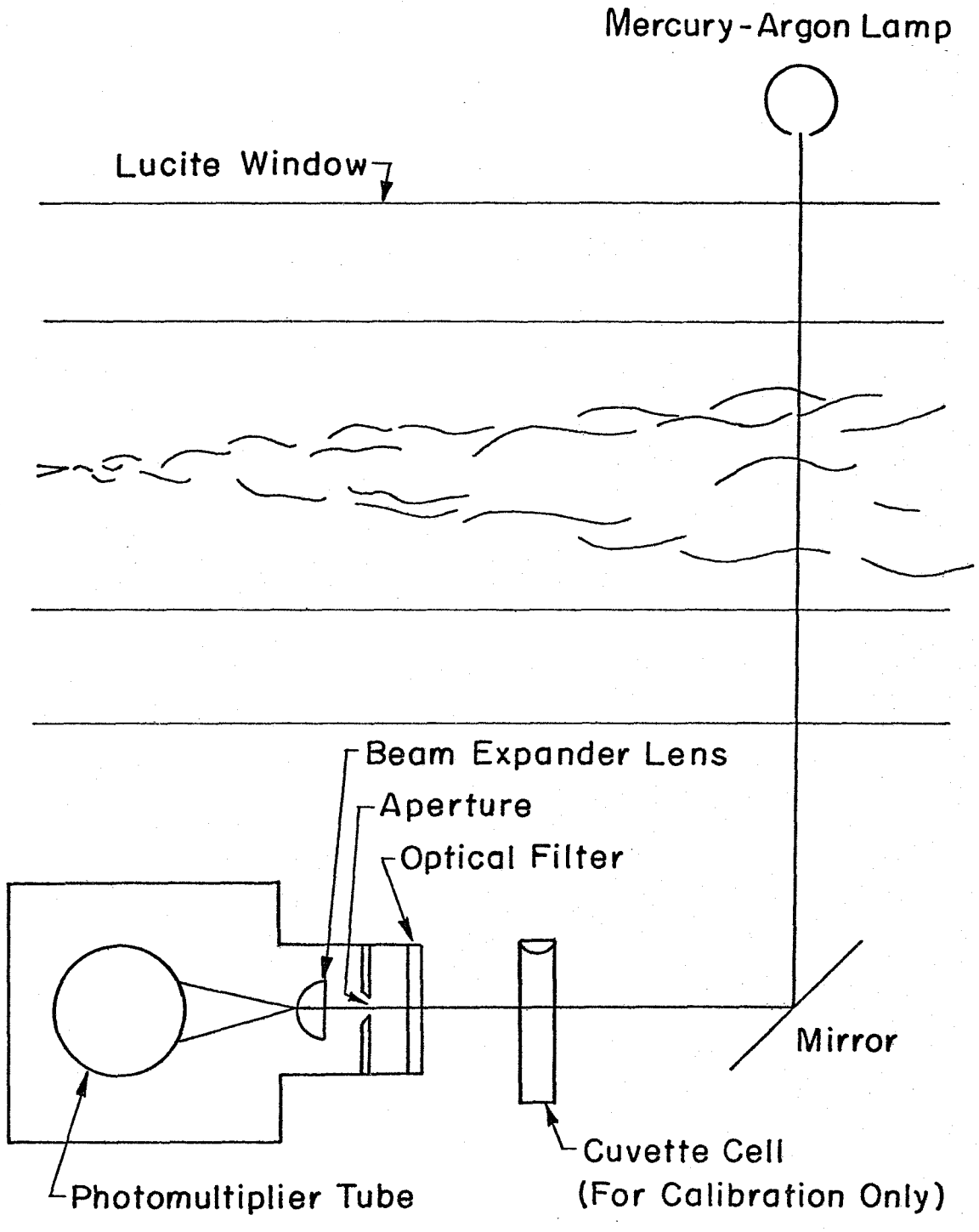

FIG. 6 OPTICAL SYSTEM

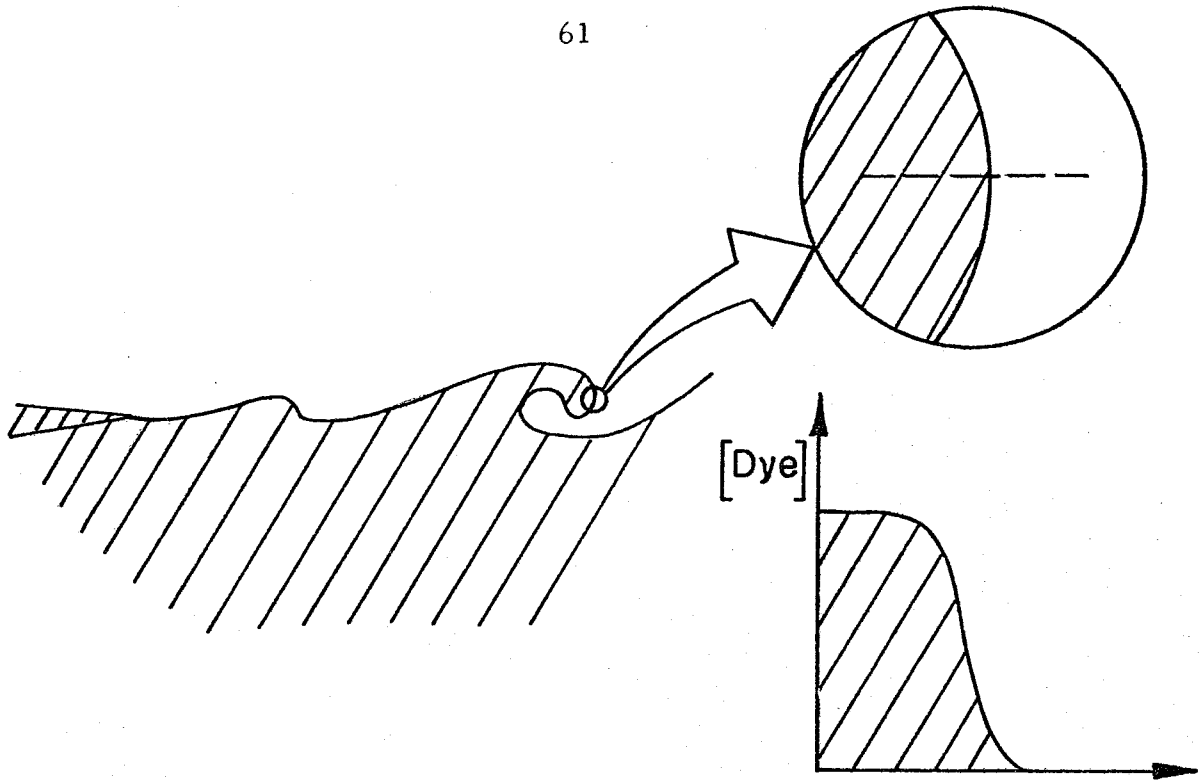

FIG. 7 INERT DYE INTERFACE

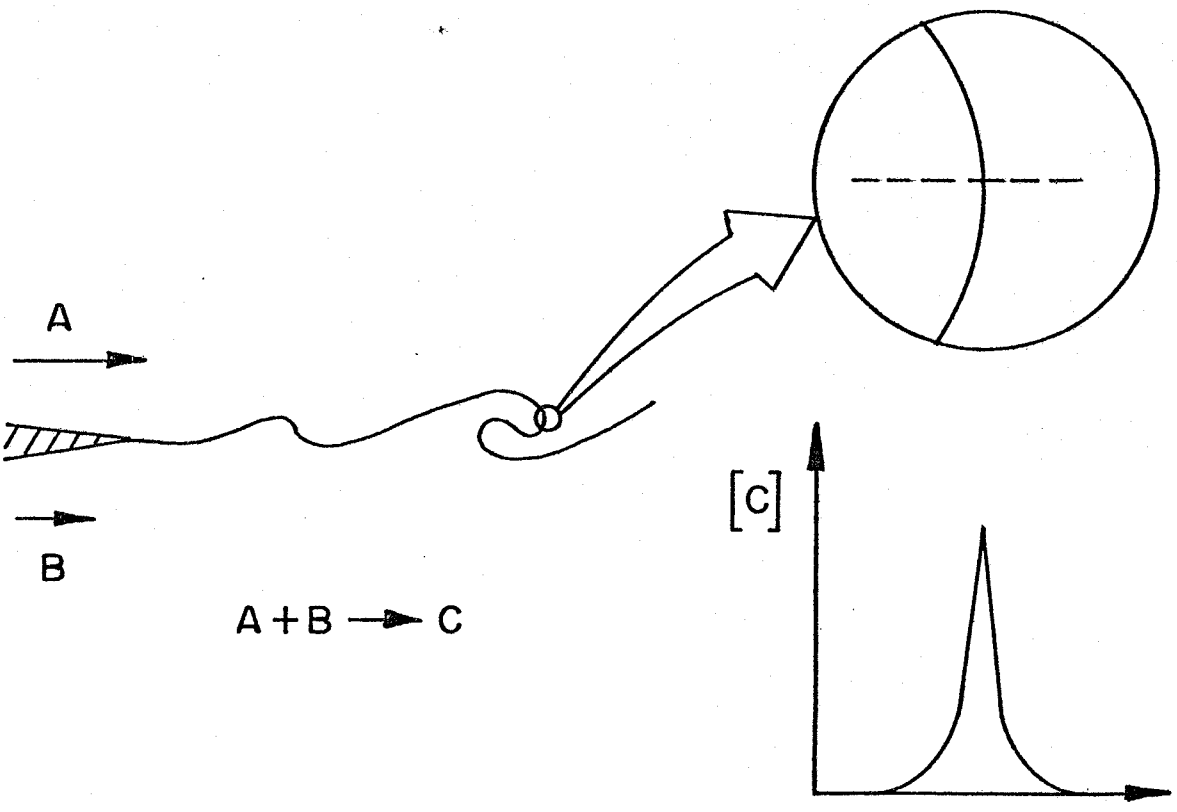

FIG. 8 REACTION INTERFACE

FIG. 9 SIDE VIEW OF THE REACTING LAYER, U_I = 37 cm/sec, r = .36

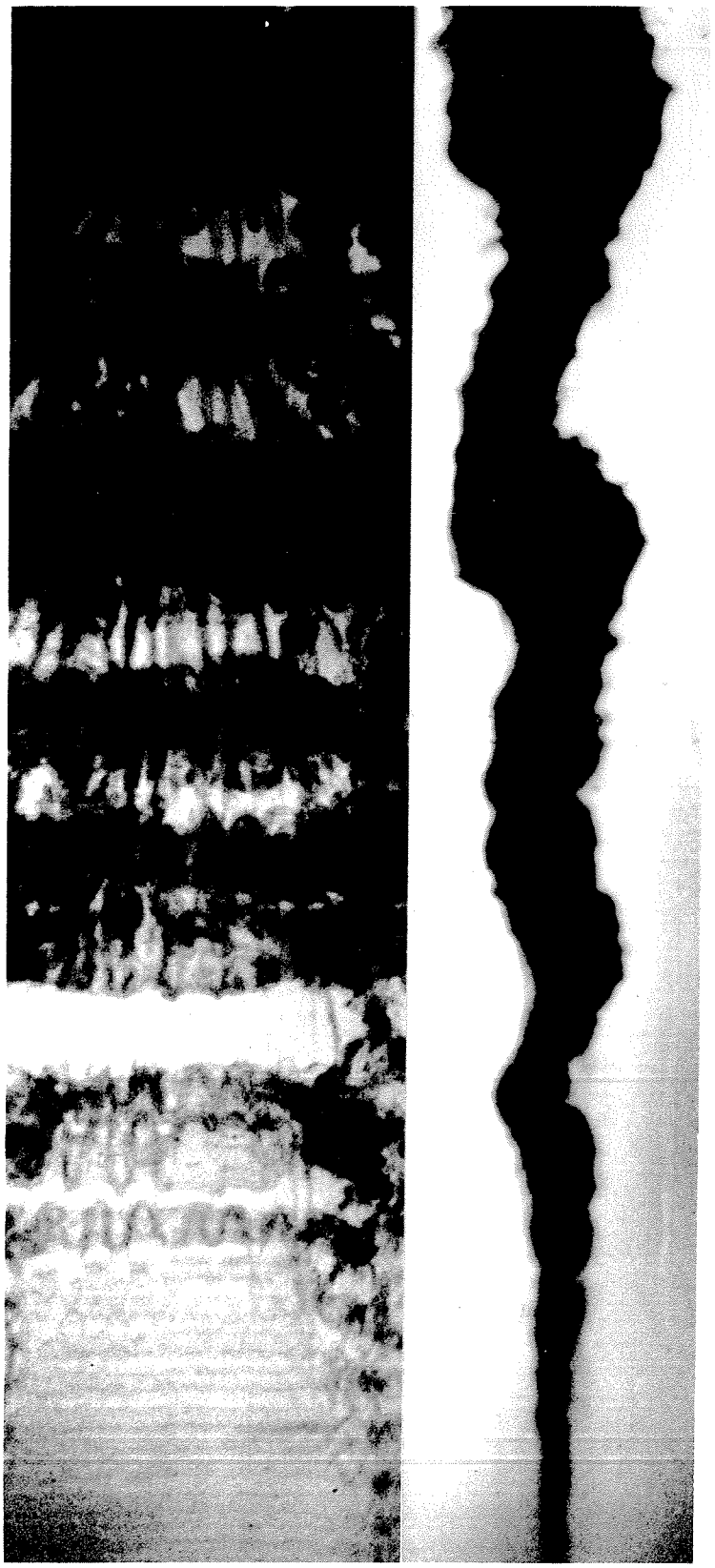

FIG. 10 SIMULTANEOUS SIDE AND PLAN VIEWS, $U_j = 50$ cm/sec, $r = .4$

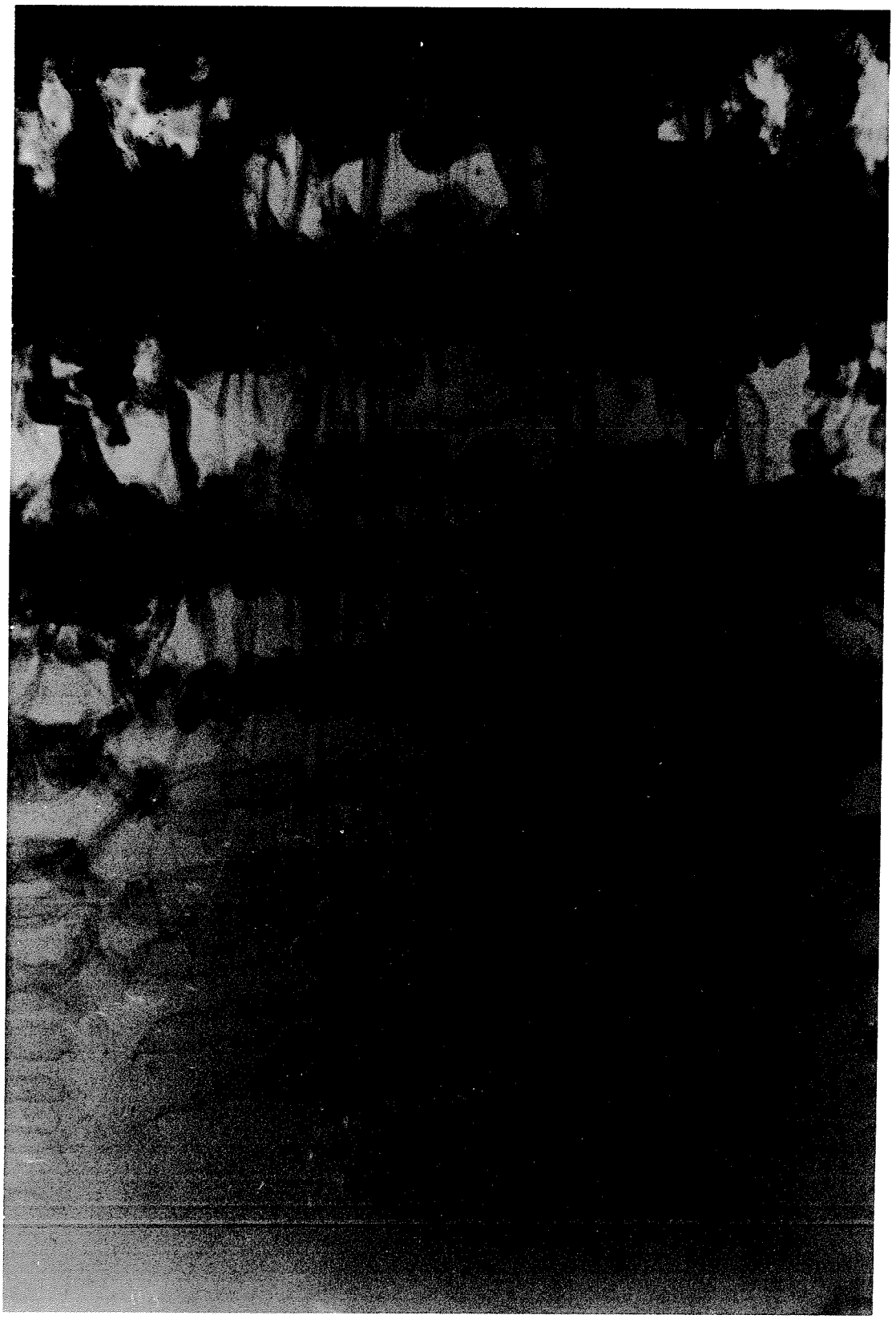

FIG. 11 CLOSEUP OF WIGGLE FORMATION, $U_\infty = 49\,cm/sec$, $r = .43$

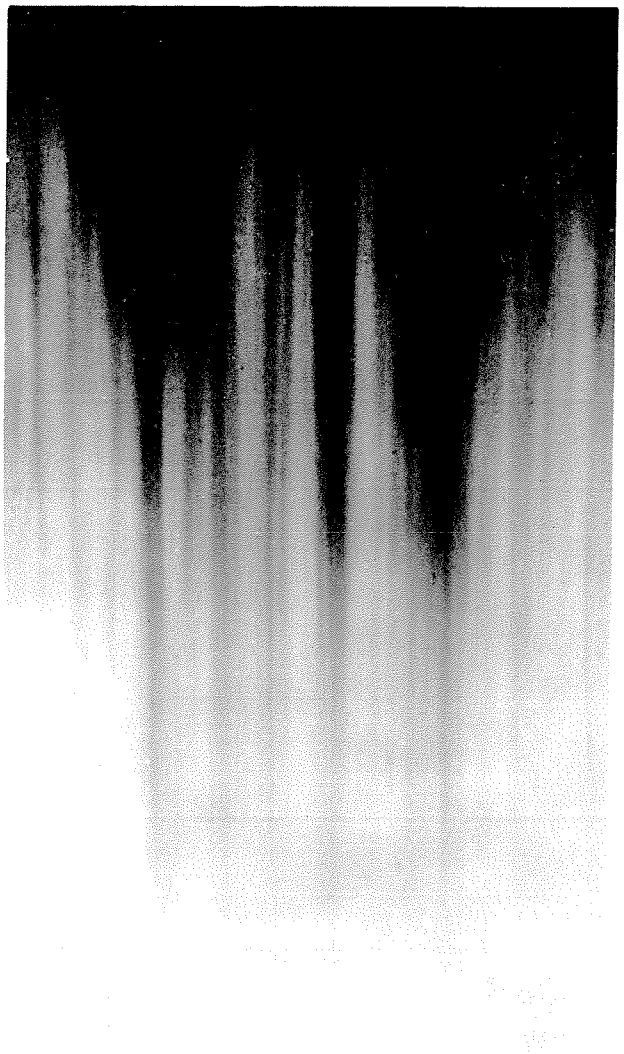

FIG. 12 TIME EXPOSURE OF THE PLAN VIEW, $U_1 = 38\,cm/sec, r = .38$

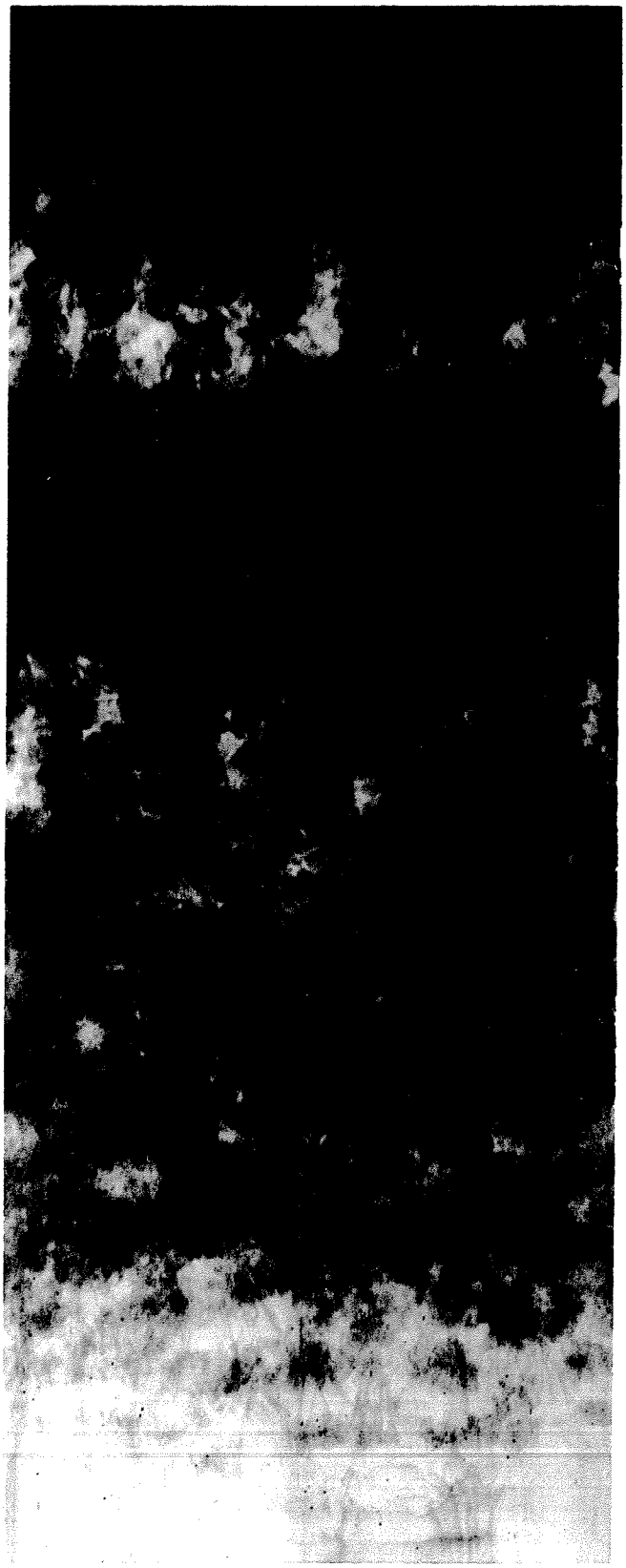

FIG. 13 SHEAR LAYER AT LARGE REYNOLDS NUMBER, $U_j = 96$ cm/sec, $r = .37$

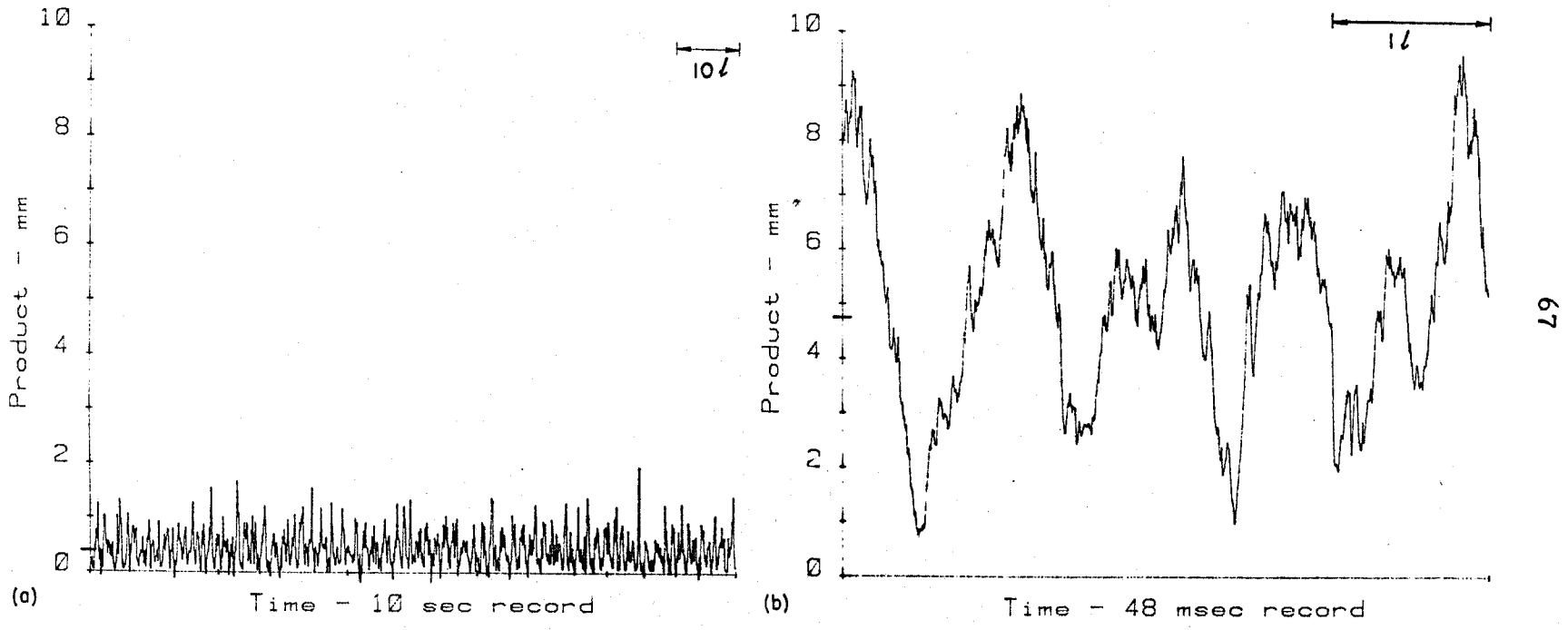

FIG. 14 PRODUCT TIME HISTORIES OF THE SHEAR LAYER

(a) $U_1 = 35$ cm/sec, $r = .36$, $x = 14$cm

(b) $U_1 = 257$ cm/sec, $r = .35$, $x = 15$cm

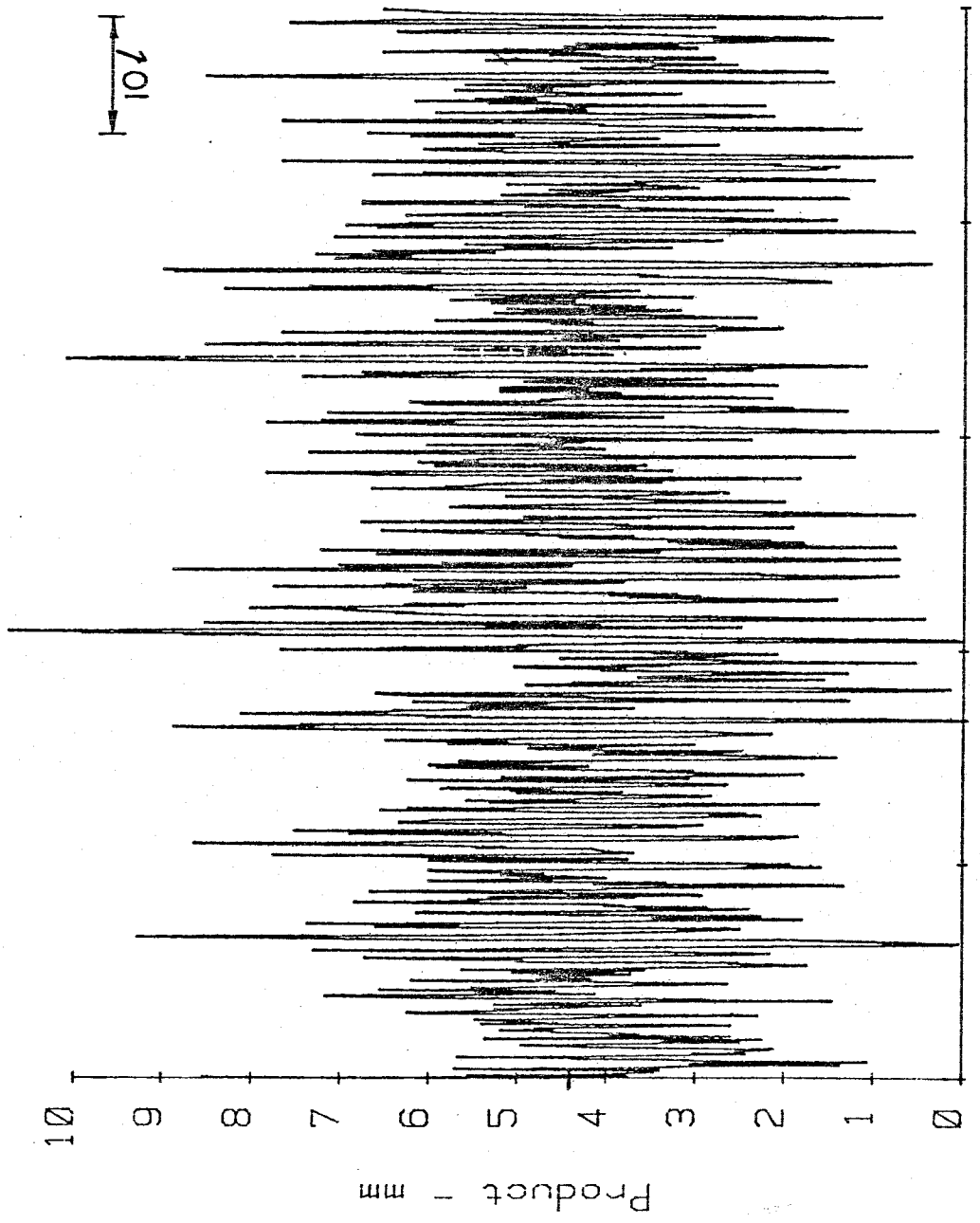

FIG.15 COMPRESSED TIME HISTORY, U_1= 465 cm/sec, r=.37, x=14cm

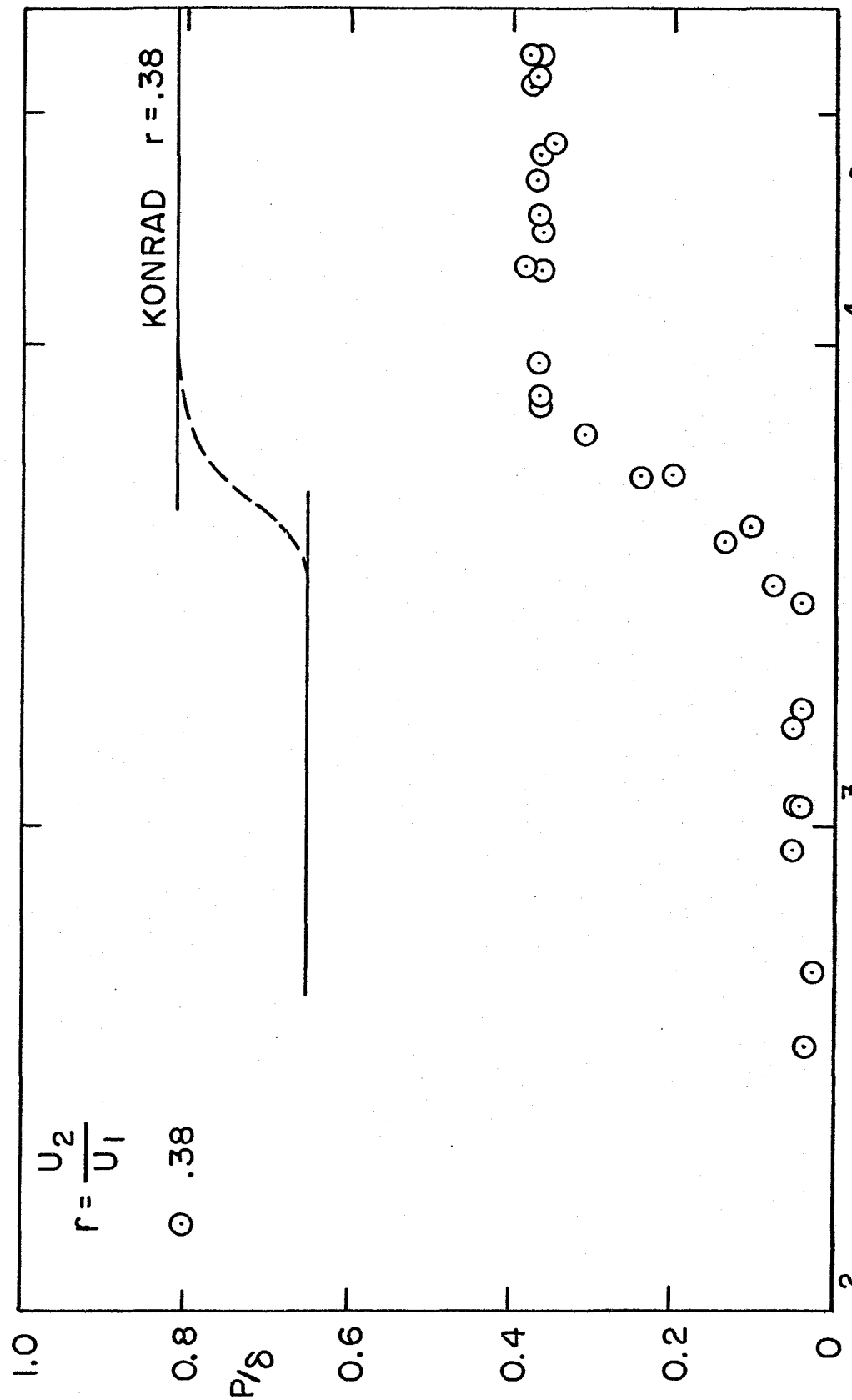

FIG. 16 DEPENDENCE OF MIXING ON LARGE SCALE REYNOLDS NUMBER

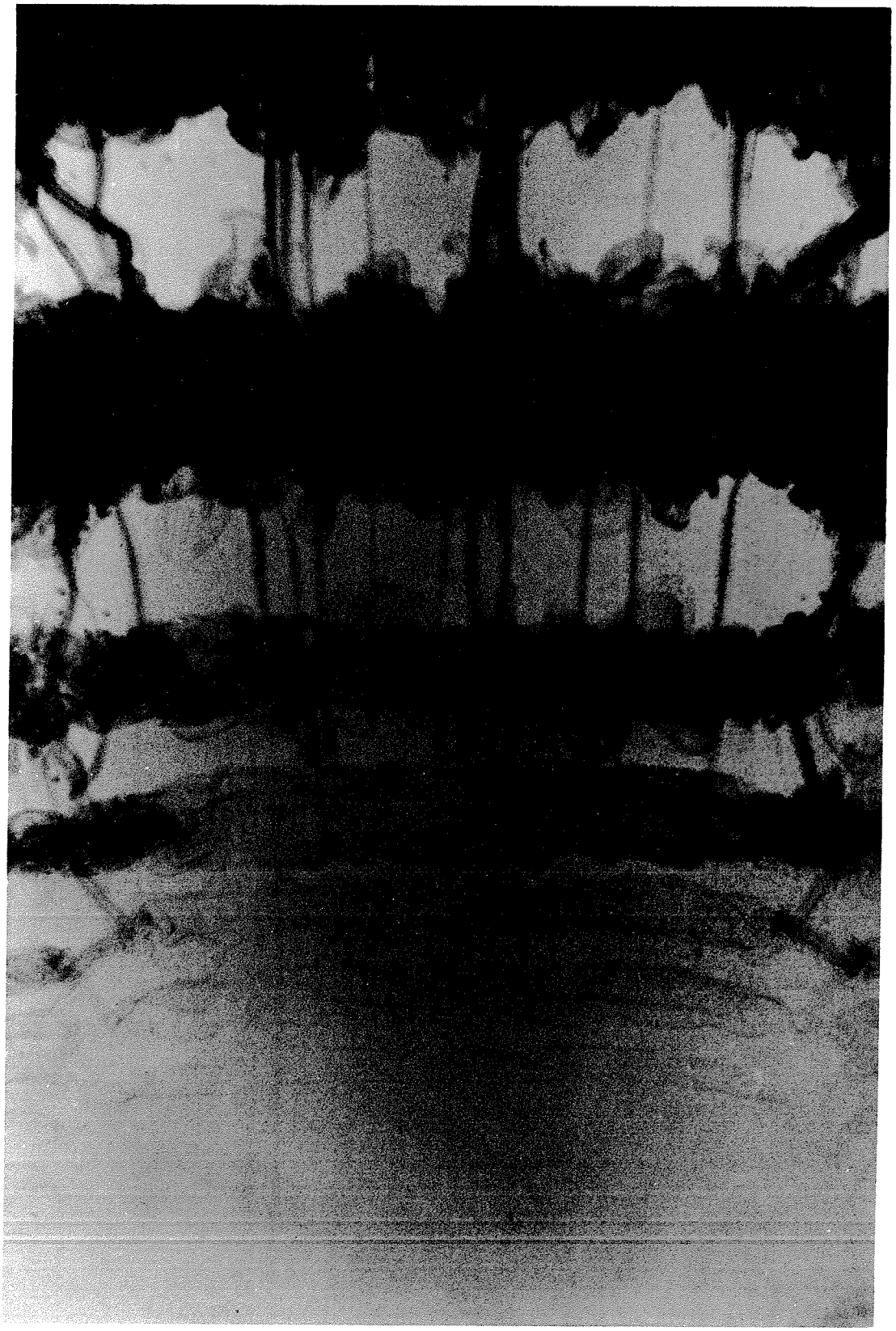

FIG. 17 PLAN VIEW OF MIXING TRANSITION, $U_1 = 43$ cm/sec, $r = .38$

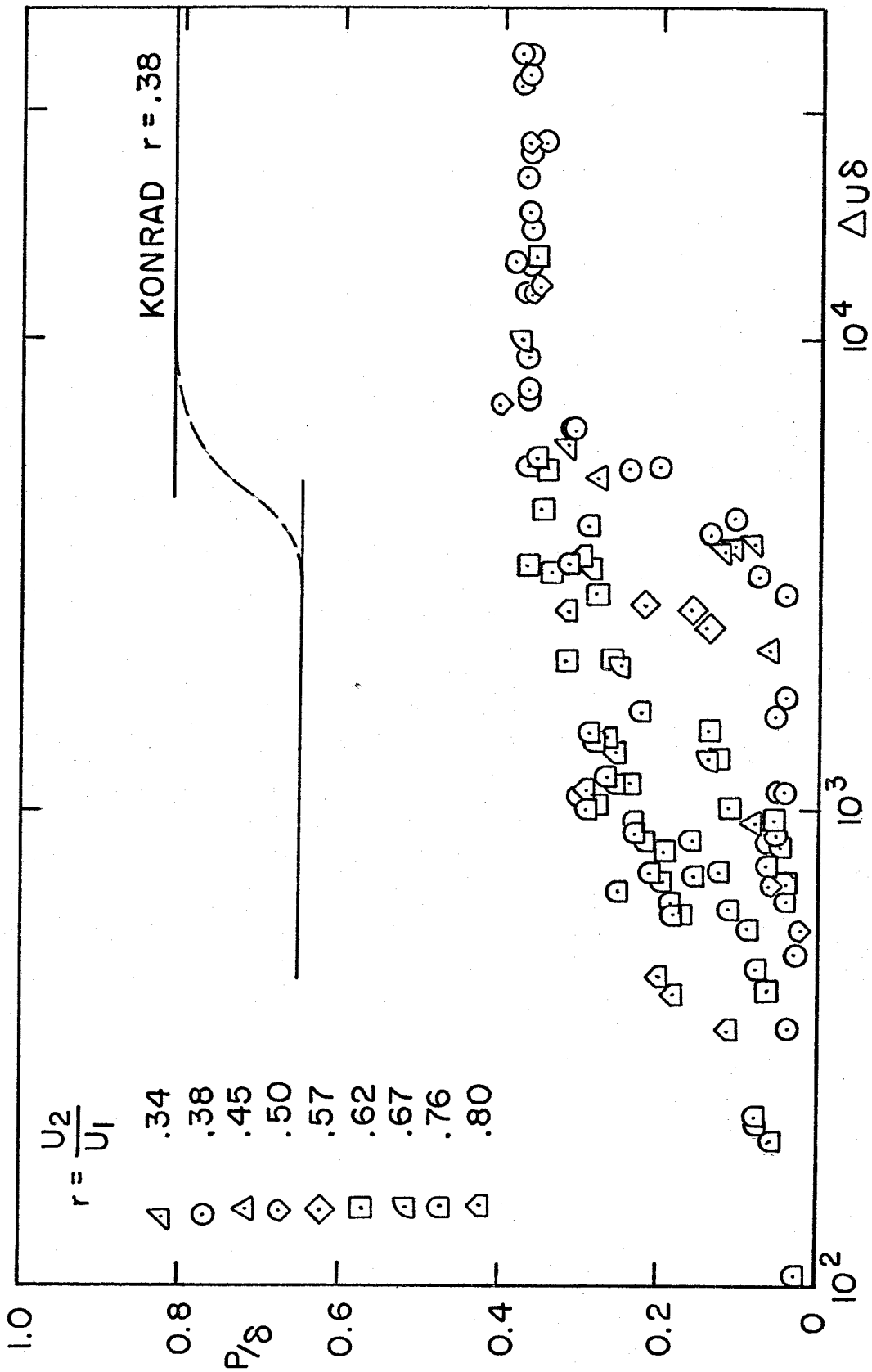

FIG. 18 EFFECT OF VELOCITY RATIO ON MIXING TRANSITION

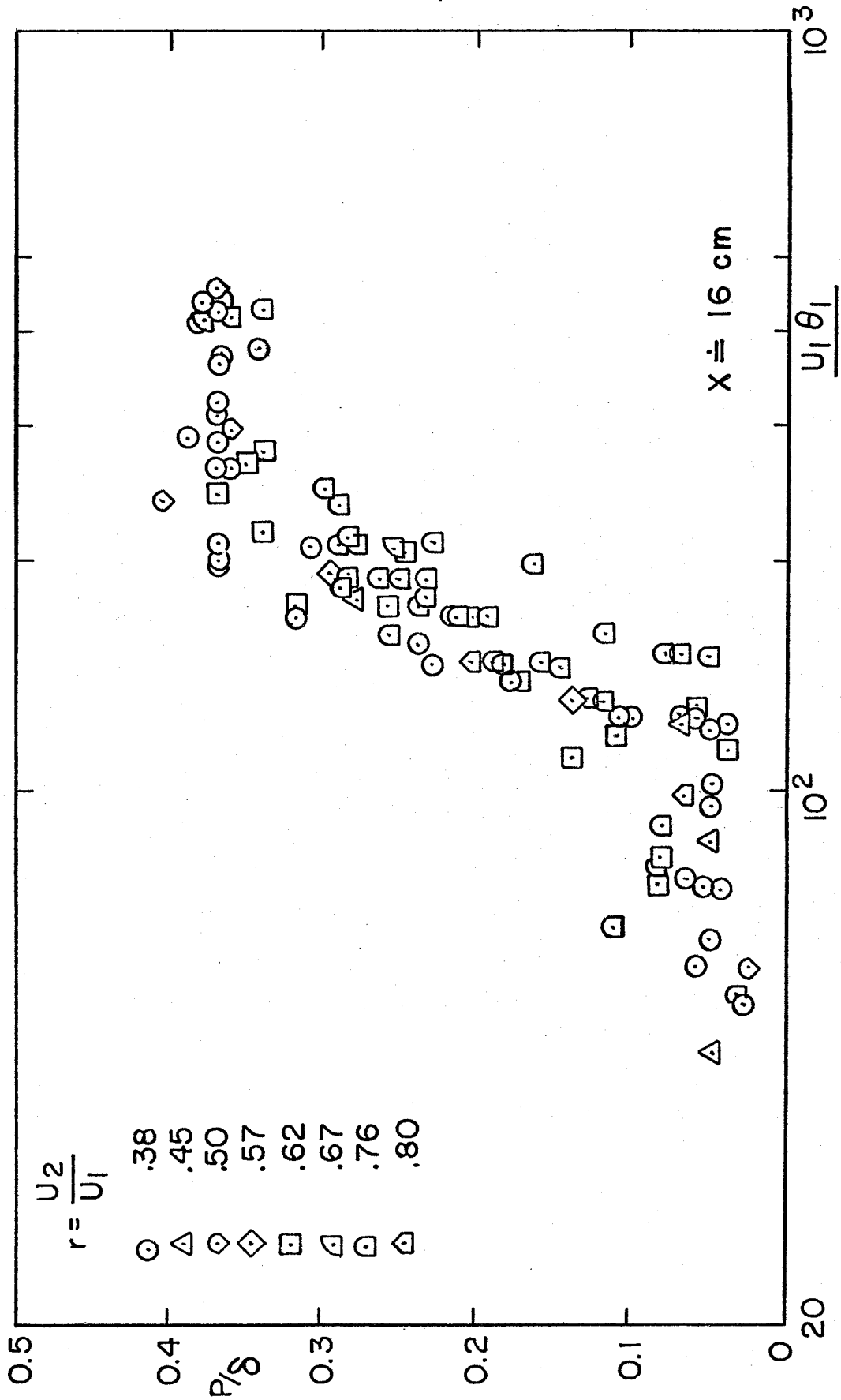

FIG.19 DEPENDENCE OF MIXING ON INITIAL REYNOLDS NUMBER

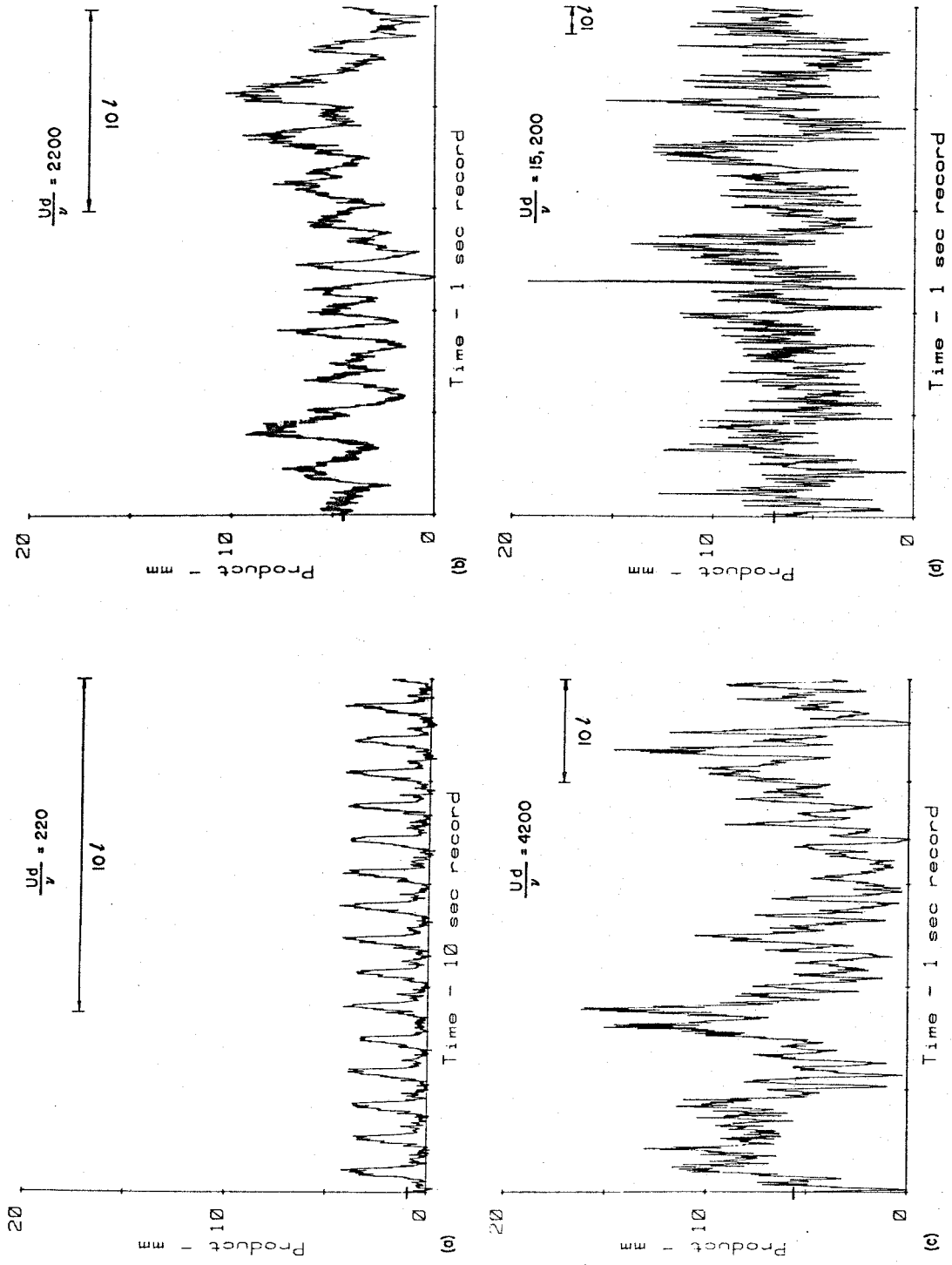

FIG. 20 PRODUCT TIME HISTORIES OF THE THICK WAKE, x = 8.5 cm

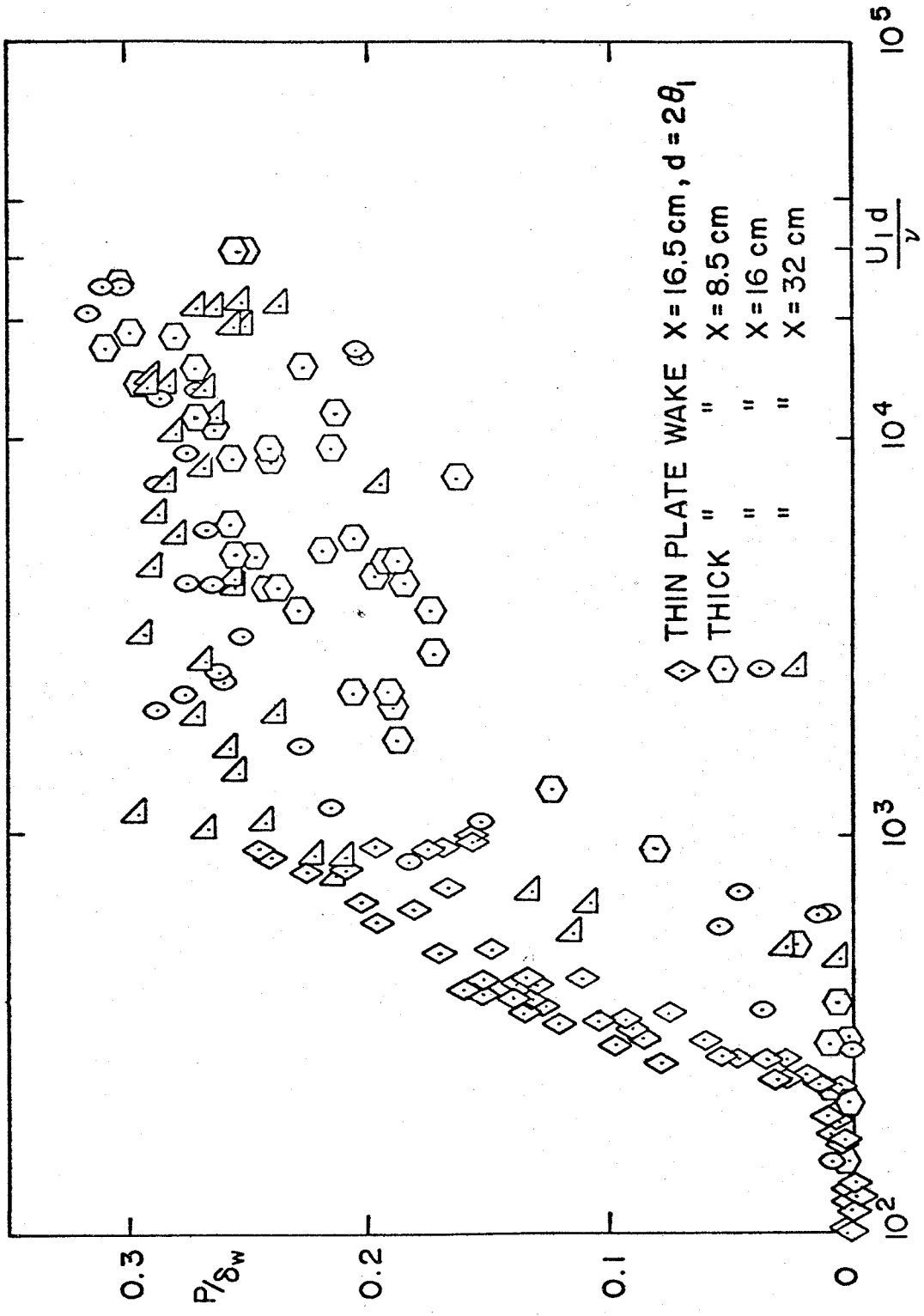

FIG. 21 DEPENDENCE OF MIXING ON THE WAKE REYNOLDS NUMBER

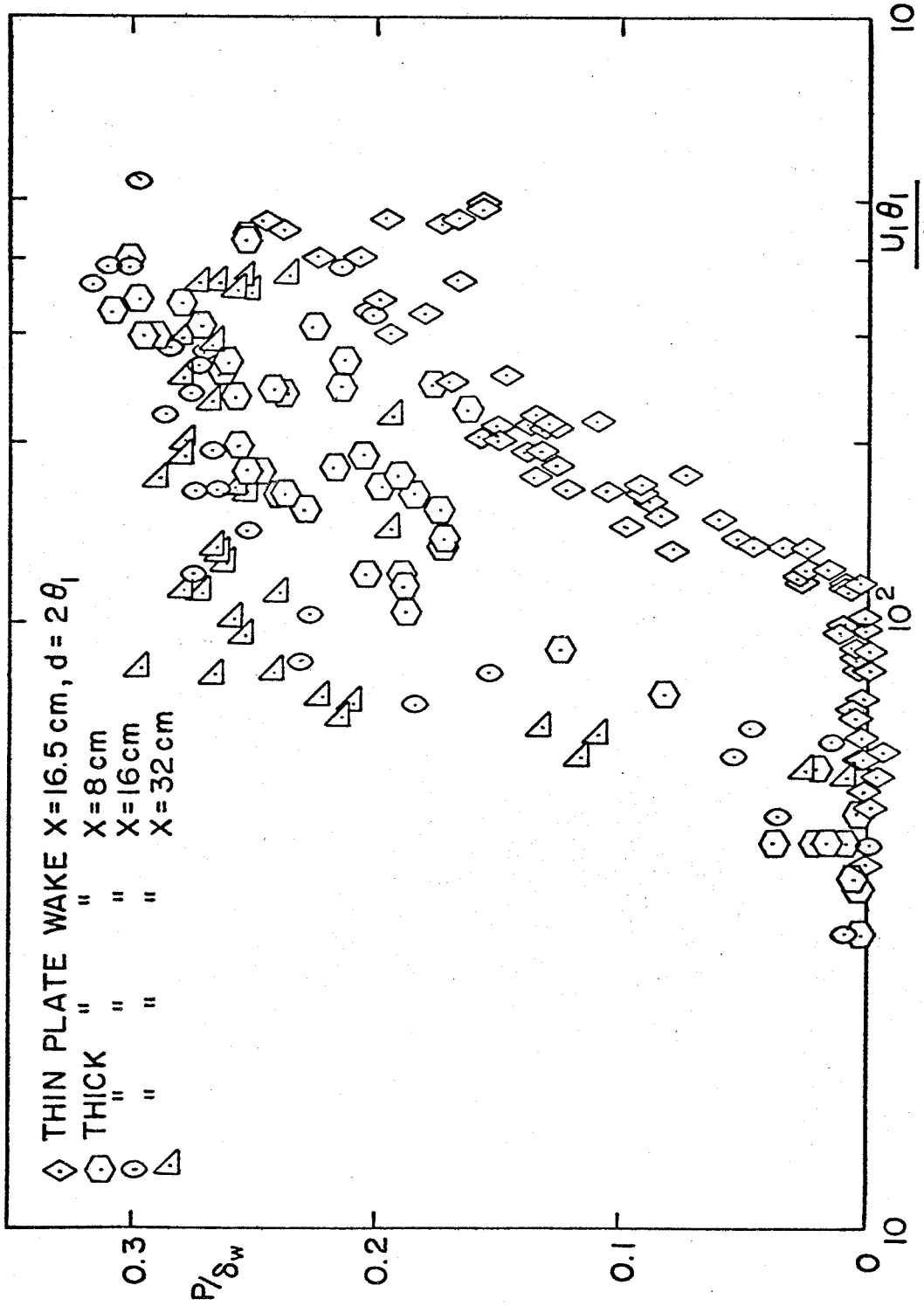

FIG. 22 DEPENDENCE OF WAKE MIXING ON INITIAL REYNOLDS NUMBER

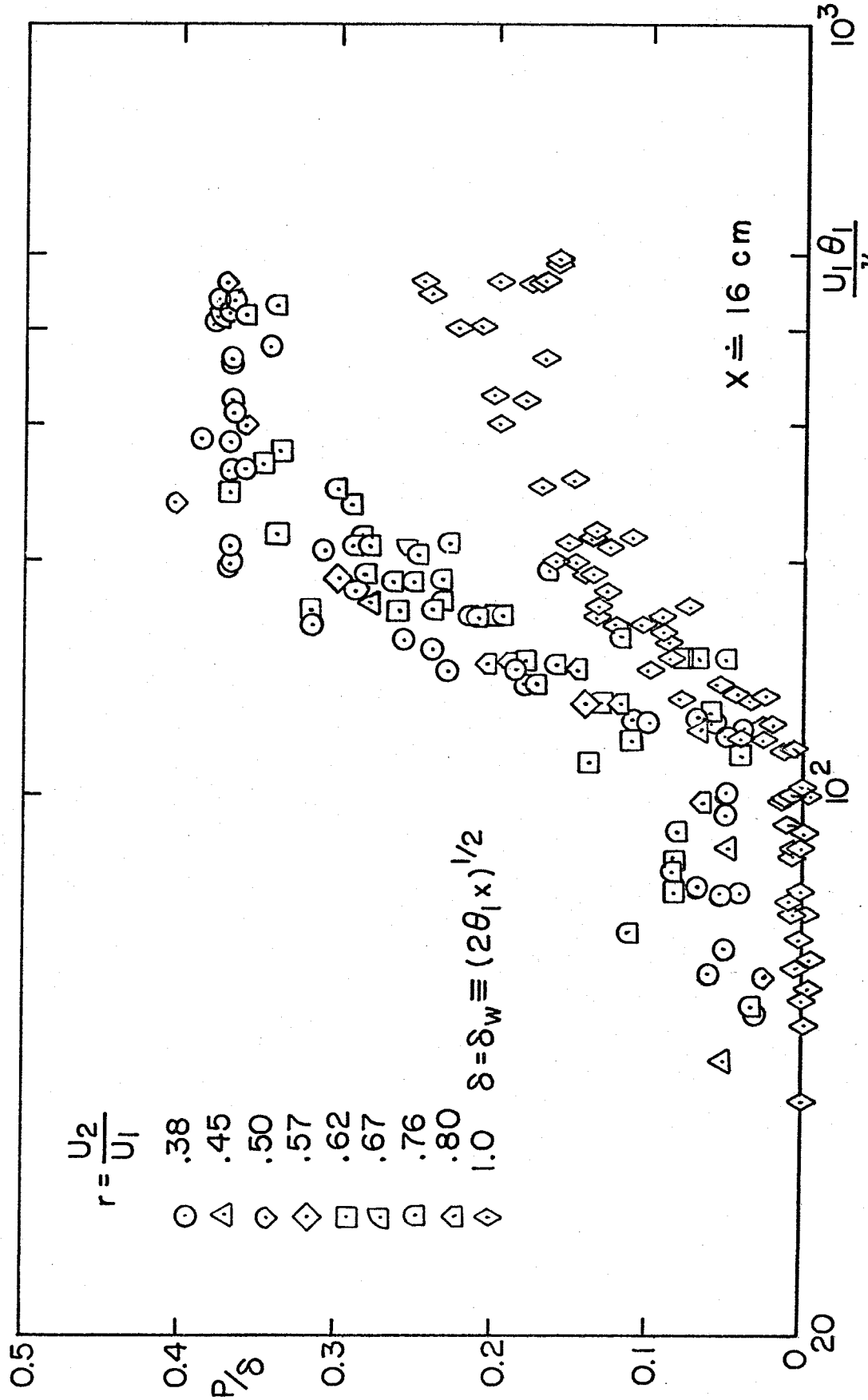

FIG. 23 EFFECT OF INITIAL REYNOLDS NUMBER ON THE SHEAR LAYER AND "THIN" WAKE

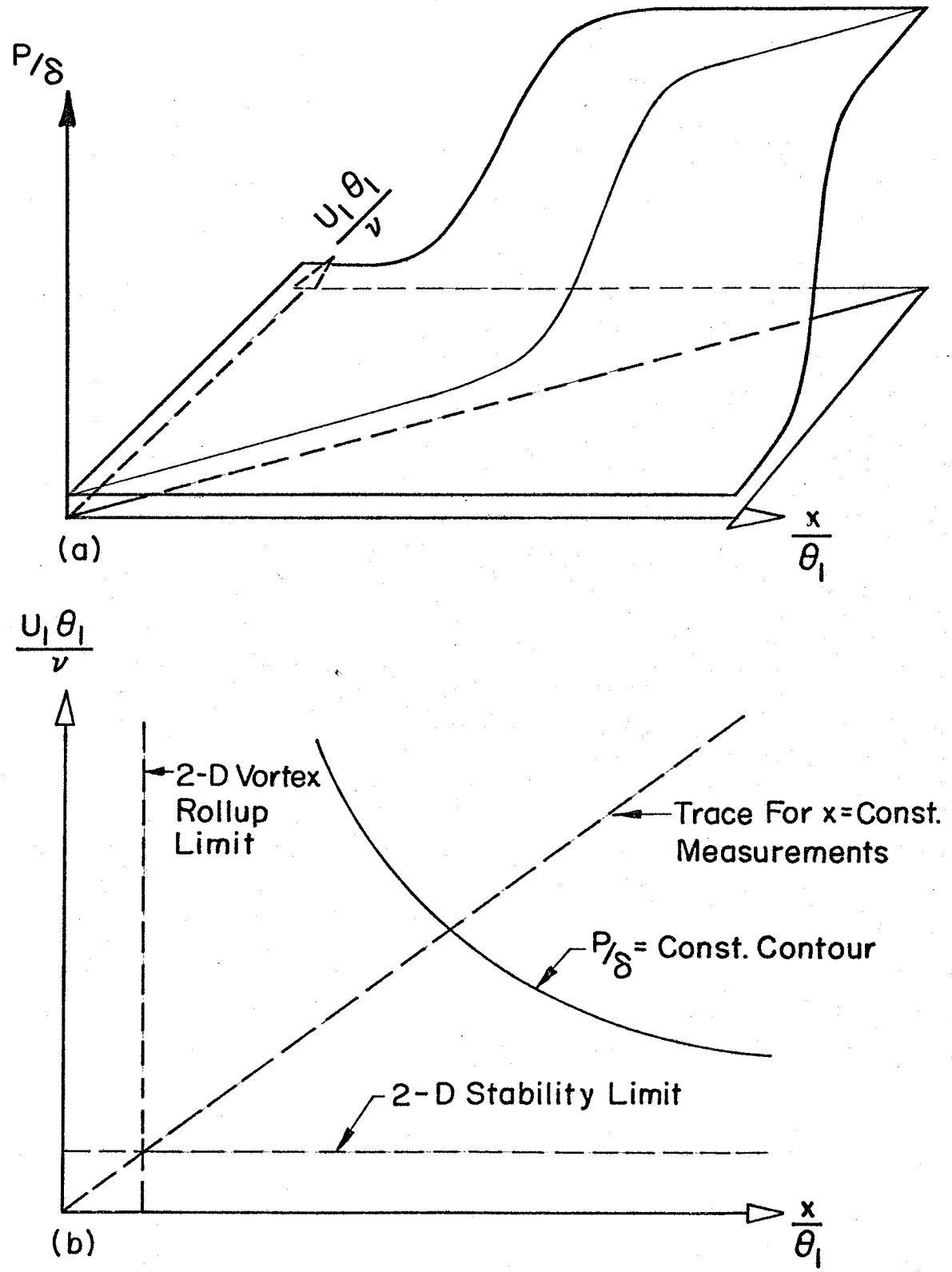

FIG. 24 SPECULATIVE EFFECT OF INITIAL CONDITIONS ON THE MIXING TRANSITION